Naval Surface Warfare Center
Carderock Division
West Bethesda, MD 20817-5700

A Stock Propeller Design for the High Speed Sealift Hybrid Contra-Rotating Shaft-Pod, Model 5653-3A

by

Jessica J. Geisbert

Seth D. Schroeder

20080616 068

REPORT DOCUMENTATION PAGE

Public reporting burden for this collection of information is estimated to average 1 hour per response, including the time for reviewing instructions, searching existing data sources, gathering and maintaining the data needed, and completing and reviewing the collection of information. Send comments regarding this burden estimate or any other aspect of this collection of information, including suggestions for reducing this burden, to Washington Headquarters Services, Directorate for Information Operations and Reports, 1215 Jefferson Davis Highway, Suite 1204, Arlington, VA 22202-4302, and to the Office of Management and Budget, Paperwork Reduction Project (0704-0188), Washington, DC 20503.

1. AGENCY USE ONLY (Leave Blank)	2. REPORT DATE	3. REPORT TYPE AND DATES COVERED
	January 2008	Final, March 2008

4. TITLE AND SUBTITLE

A Stock Propeller Design for the High Speed Sealift Hybrid Contra-Rotating Shaft-Pod, Model 5653-3A

5. FUNDING NUMBERS

07-1-2125-146
08-1-2125-144
08-1-2125-146

6. AUTHOR(S)

Jessica J. Geisbert
Seth D. Schroeder

7. PERFORMING ORGANIZATION NAME(S) AND ADDRESS(ES)

Resistance and Propulsion Division, Code 5800
NSWC, Carderock Division
9500 MacArthur Blvd.
West Bethesda, MD 20817-5700

8. PERFORMING ORGANIZATION REPORT NUMBER

NSWCCD-50-TR-2008/003

9. SPONSORING / MONITORING AGENCY NAME(S) AND ADDRESS(ES)

Commander, PMS 385
Naval Sea Systems Command
1333 Isaac Hull Ave, SE
Washington Navy Yard, DC 20375-2501

10. SPONSORING / MONITORING AGENCY REPORT NUMBER

11. SUPPLEMENTARY NOTES

12.a DISTRIBUTION / AVAILIBILITY STATEMENT

Approved for Public Release - Distribution is Unlimited

12.b DISTRIBUTION CODE

13. ABSTRACT (Maximum 200 words)

A stock propulsor has been designed for the High Speed Sealift Hybrid Contra-Rotating Shaft-Pod. The forward propeller of the contra-rotating set is a standard shaft and strut mounted propeller. The aft propeller is driven by a COTS tractor pod. The full power speed of this design is 39 knots.

The final design has a 21.5 foot diameter, five-bladed propeller forward and a 17 foot diameter, seven-bladed propeller aft. Both the forward and aft propellers operate at 113 RPM. Calculations predict that the design will achieve the 39 knot target speed without significant thrust breakdown. A final propulsive coefficient of 0.716 is predicted at 39 knots with 191,500 DHP (143 MW). A propulsive coefficient of 0.64 was measured for the same hull form with four shafts and struts at 39 knots and 231,300 DHP (172 MW). Therefore, this design predicts a 17% decrease in the required DHP.

These propellers are currently being manufactured at model scale for open water and powering tests.

16. SUBJECT TERMS

PROPELLERS, CONTRA-ROTATING, PODS

15. NUMBER OF PAGES

54

16. PRICE CODE

17. SECURITY CLASSIFICATION OF REPORT	18. SECURITY CLASSIFICATION OF THIS PAGE	19. SECURITY CLASSIFICATION OF ABSTRACT	20. LIMITATION OF ABSTRACT
UNCLASSIFIED	UNCLASSIFIED	UNCLASSIFIED	SAME AS REPORT

(THIS PAGE INTENTIONALLY LEFT BLANK)

CONTENTS

LIST OF TABLES

Page

LIST OF FIGURES

Page

NOMENCLATURE

A_p — Projected blade area

BSS — Baseline Shaft and Strut

c — chord length

C_L — Lift coefficient of section, $\dfrac{\text{Lift}}{\frac{1}{2}\rho V_{rel}^2 c}$

COTS — Commercial Off The Shelf

D — Diameter

deg — degrees

DHP — Delivered Horsepower

EAR — Expanded Area Ratio

EHP — Effective Horsepower

f — camber

ft — foot, feet

g — gravitational constant

G — Non-dimensional circulation

h — propeller depth

hp — horsepower

HSS — High Speed Sealift

in — inches

JHSS — Joint High Speed Sealift

J_S — Ship advance coefficient, $\dfrac{V_S}{nD}$

kts — knots

K_T — Thrust coefficient, $\dfrac{\text{Thrust}}{\rho n^2 D^4}$

K_Q — Torque coefficient, $\dfrac{\text{Torque}}{\rho n^2 D^5}$

lb — pounds

LDV — Laser Doppler Velocimetry

LH — Left Handed

LOA — Length Overall

LT — Long Tons

LWL — Waterline Length

m — meters

MW — Megawatts

n — revolutions per second

NSWCCD — Naval Surface Warfare Center, Carderock Division

p — pitch

p_0 — atmospheric pressure

p_v — vapor pressure of water

P — Power

PC — Propulsive Coefficient, $\dfrac{\text{EHP}}{\text{DHP}}$

psi — pounds per square inch

r — propeller radius at a section

R — Overall propeller radius

RH — Right Handed

RPM — Revolutions Per Minute

SLA — Stereolithography Apparatus

t — thickness

t — thrust deduction

T — Thickness at the root

V_a — Axial velcoity in propeller plane, $V_A = V_S(1-w)$

V_c — Velocity tangent to the blade surface in the chordwise direction

V_n — Velocity normal to the blade surface

V_{rel}	Relative velocity	$\sigma_{0.7R}$	Burrill cavitation number,
V_S	Ship speed		$\dfrac{p_0 - p_v + \rho gh}{\frac{1}{2}\rho\left(V_A^2 + (0.7\pi nD)^2\right)}$
w	wake fraction		
Z	Number of blades	τ_c	Burrill thrust loading
δ	incremental mean line slope		coefficient, $\dfrac{\text{Thrust}}{\frac{1}{2}\rho A_p\left(V_A^2 + (0.7\pi nD)^2\right)}$
η_B	behind efficiency		
ρ	mass density		

(THIS PAGE INTENTIONALLY LEFT BLANK)

ABSTRACT

A stock propulsor has been designed for the High Speed Sealift Hybrid Contra-Rotating Shaft-Pod. The forward propeller of the contra-rotating set is a standard shaft and strut mounted propeller. The aft propeller is driven by a COTS tractor pod. The full power speed of this design is 39 knots.

The final design has a 21.5 foot diameter, five-bladed propeller forward and a 17 foot diameter, seven-bladed propeller aft. Both the forward and aft propellers operate at 113 RPM. Calculations predict that the design will achieve the 39 knot target speed without significant thrust breakdown. A final propulsive coefficient of 0.716 is predicted at 39 knots with 191,500 DHP (143 MW). A propulsive coefficient of 0.64 was measured for the same hull form with four shafts and struts at 39 knots and 231,300 DHP (172 MW). Therefore, this design predicts a 17% decrease in the required DHP.

These propellers are currently being manufactured at model scale for open water and powering tests.

ADMINISTRATIVE INFORMATION

INTRODUCTION

This report presents the design of a custom stock propulsor for the High Speed Sealift Contra-Rotating Shaft-Pod. It first summarizes the propulsion studies done under the High Speed Sealift (HSS) program, and then presents the design requirements and outlines the propulsor design process. The inputs, method and results of the parametric study are discussed. The 3D lifting surface code is discussed and the results are presented. Lastly, the report presents the final design. This design will be used for open water and powering tests on Model 5653-3, a 34th-scale powering model.

BACKGROUND

This work was performed under the High Speed Sealift (HSS) program. The scope of the HSS program includes[1]:

- developing reliable design methods and tools,
- comparing performance analyses with experimental results for predictive accuracy,
- identifying experimental methods for the high speed operating regime,
- identifying design characteristics of benefit to High Speed Sealift.

A notional, monohull high speed sealift ship is being studied under the HSS program. This ship was originally named the Joint High Speed Ship, or JHSS. The notional mission of the JHSS was to carry military cargo at 36 to 39 knots over a range of 8000 nautical miles[1].

Three different propulsion systems were tested at model scale on the JHSS hull form: four shaft and strut mounted propellers, four axial flow waterjets, and four mixed flow waterjets [1]. The stern of the JHSS hull form was altered for each propulsion system. Figure 1 shows the three different JHSS hull forms[1].
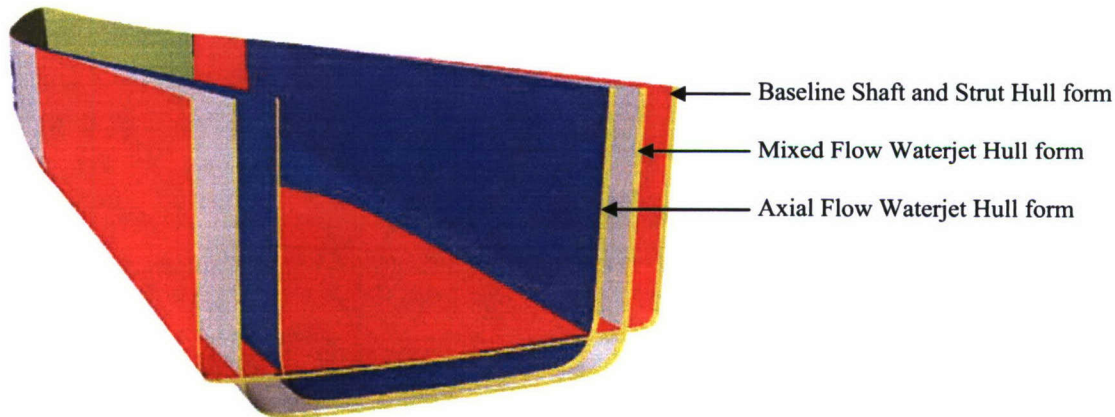
Figure 1. The three different JHSS hull forms.

The JHSS Baseline Shaft and Strut (BSS) hull form has four shafts and struts, each with a 7.5 in diameter propeller (21.33 ft diameter full scale). Model scale powering tests with stock propellers revealed that the JHSS BSS hull performed with a PC of approximately 0.64 at 39 knots, 231,300 DHP (172 MW) and 173 RPM [2].

Contra-rotating propulsors and commercial off the shelf (COTS) azimuthal podded propulsors are now being considered for the JHSS BSS hull form. Contra-rotating propellers have traditionally been arranged with concentric shafts rotating in opposite directions, each shaft

[1] Dicks, Chris, "Research & Tool Development in Support of High Speed Sealift Concepts", RINA MSS Conference Presentation, (September 2007).

driving one propeller. Concentric shafts have historically introduced problems with seals, bearings, and maintenance. For this study, pods are being considered as the aft propulsor of the contra-rotating set. The forward propulsor of the set will either be a shafted propeller or a fixed pod. The pods being considered in this study are manufactured by ABB Marine & Turbocharging [3]. Using a pod as the aft propulsor of a contra-rotating set allows for the hydrodynamic benefits of contra-rotation without the shafting and gearing complexities. The pods should also give maneuvering benefits because they can rotate azimuthally.

This contra-rotating pod configuration has been used before. The Shin Nihonkai Ferry used a diesel-electric hybrid contra-rotating system with a skeg mounted propeller forward and a pod aft [4]. Pods have also been widely used on cruise ships.

CONCEPT SELECTION

Model 5653-3, the JHSS Baseline Shaft and Strut (BSS) hull form, is being used for this design [2]. The -3 suffix affixed to the model number denotes the installation of a gooseneck bow bulb.

HULL FORM

Particulars for the model at design displacement are shown in Table 1 [2]. Figure 2 shows a picture of the model [5]. The scale ratio for the model is 34.121.

Table 1. Hull form particulars of Model 5653-3.

	Full Scale without Pods	Model Scale without Pods	Full Scale with Pods	Model Scale with Pods
LOA	982.4 ft	28.79 ft	982.4 ft	28.79 ft
LWL	977.8 ft	28.66 ft	978.2 ft	28.67 ft
Beam	104.9 ft	3.075 ft	104.9 ft	3.075 ft
Draft	28.85 ft	0.8455 ft	28.73 ft	0.8421 ft
Displacement	36491 tons	2004 lbs	36491 tons	2004 lbs
Trim	0 deg	0 deg	0 deg	0 deg

Figure 2. A picture of Model 5653-3.

CONFIGURATIONS

Model scale powering tests of Model 5653-3, the JHSS BSS hull, revealed that 172 MW of delivered power was needed to achieve 39 knots [2]. It was assumed that by incorporating pods and contra-rotation, less power would be needed to propel the ship to 39 knots.

The maximum power supported by the off the shelf pods is currently 25 MW (33,530 hp). Therefore, if no other propulsor was used to augment the power, six to seven pods would be needed to propel the ship. Because it is undesirable and unrealistic to have only pods propel the ship, configurations that also incorporated different types of propulsors (shafts and struts, fixed pods) were explored. A few of the preliminary configurations that were considered are shown in Figure 3.
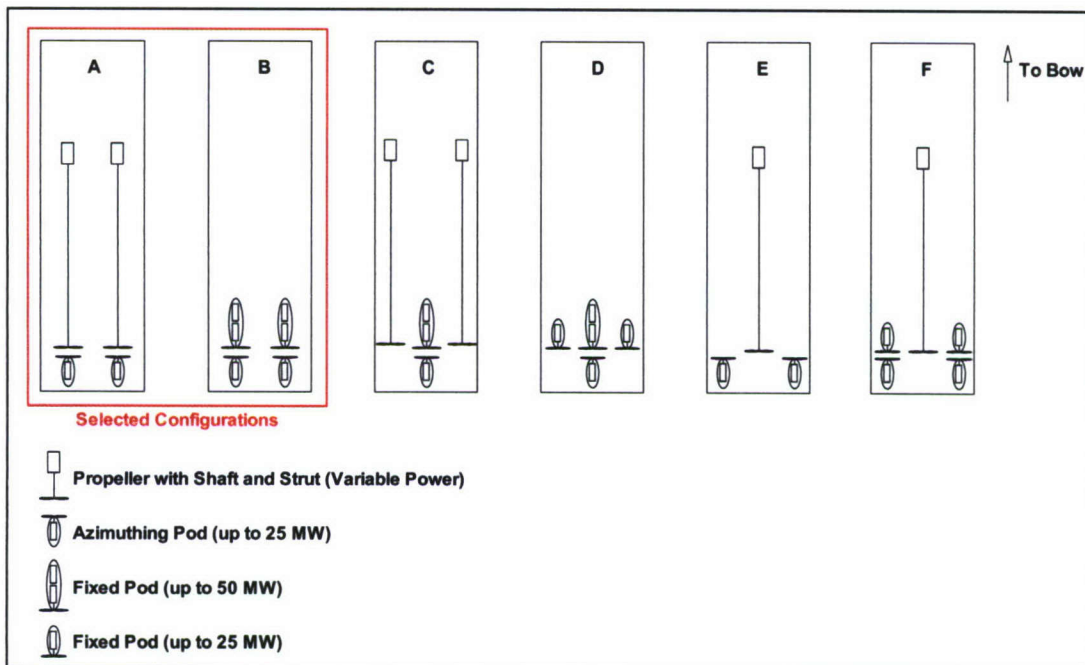

Figure 3. Some of the configurations considered for the HSS ship.

For the configurations above, it was assumed that the shaft and strut mounted propellers could be driven by prime movers with flexible ranges of power and RPM. The 50 MW (67,050 hp) fixed pods would contain two 25 MW motors connected in series.

Configurations A and B in Figure 3 were chosen as the configurations on which to focus. Configuration C was rejected because three propellers cannot fit across the beam of the ship without overhang and because two azimuthing pods were desired for redundancy. Configuration D was rejected because it did not provide enough power to achieve 39 knots, it has only one azimuthing pod, and because it also has three propellers in line across the beam. Configuration E was rejected because it did not incorporate contra-rotation and because there was too much power being supplied by the center shaft. Configuration F was rejected because it also had three propellers in line across the beam.

Configuration A is referred to as the Shaft-Pod configuration while configuration B is referred to as the Dual-Pod configuration.

Shaft-Pod Configuration

The Shaft-Pod configuration has two 25 MW azimuthing pods aft and two shaft and strut mounted propellers forward. The power needed for each shaft and strut mounted propeller will be determined during the parametric study and is discussed in a later section. The total power provided to the shafts and struts will be equal to the power necessary to achieve the 39 knot target speed minus the 50 MW provided by the pods. This configuration was chosen because it utilizes contra-rotation and allows for flexibility in the power delivered to the forward blade rows. Having two azimuthing pods aft also provides maneuverability benefits.

Figures 4 through 6 show computer generated models of the Shaft-Pod configuration (provided by NSWCCD Code 5800[2]). Table 2 displays the relevant full scale geometric characteristics. In Table 2, the shaft depth is measured from the design waterline. The axial spacing is measured between the centerlines of the propellers. The transverse distance from the ship centerline is measured from the centerline of the forward propeller. The shafts and struts and pods are splayed one degree inward to better align the propellers with the flow.

---

[2] Email from Jonathan Slutsky to Jessica Geisbert on 11/20/2007
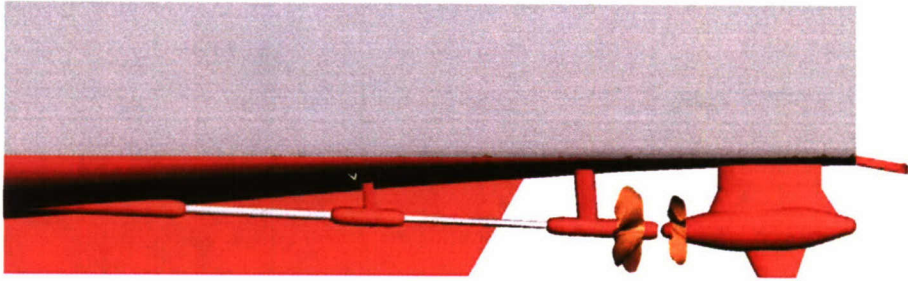
Figure 4. A side view of the Shaft-Pod configuration.
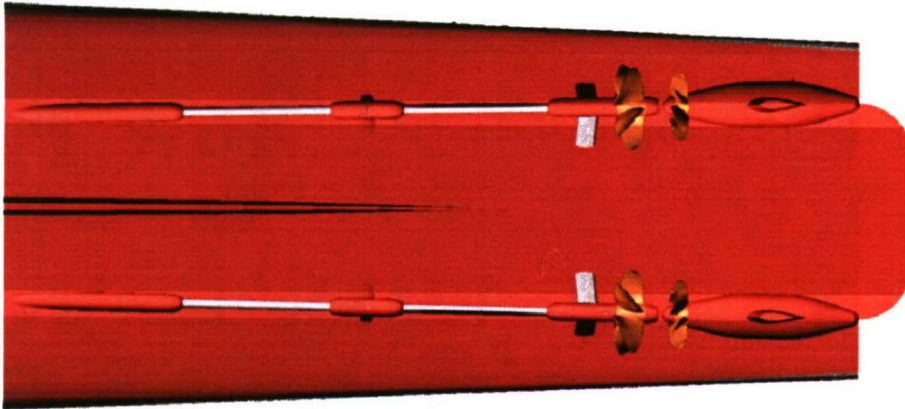
Figure 5. A bottom view of the Shaft-Pod configuration.
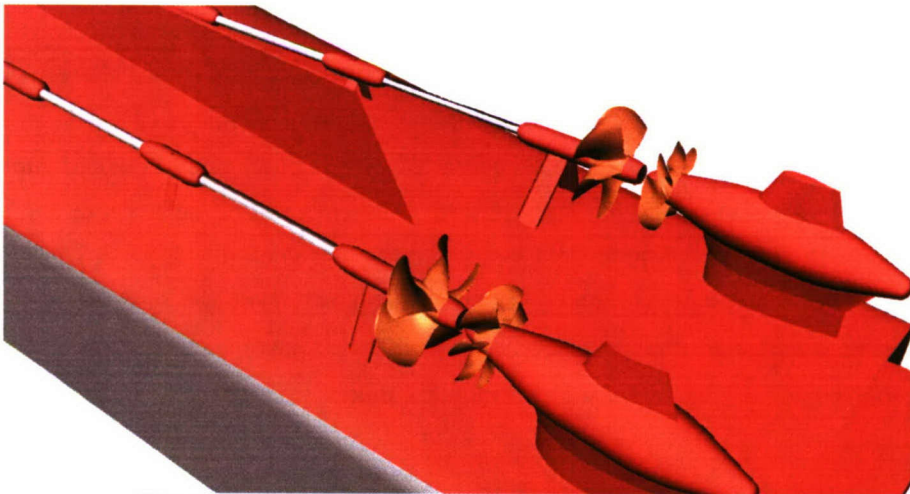
Figure 6. An isometric view of the Shaft-Pod configuration.

Table 2. The full scale particulars of the Shaft-Pod configuration.

Maximum Forward Diameter	23 ft
Tip Clearance with Maximum Forward Diameter	20 %
Forward Shaft Depth	17.5 ft
Axial Spacing	16.9 ft
Forward Propeller Shaft Angle	2.3 deg
Aft Propeller Shaft Angle	-1.6 deg
Splay Angle	1 deg
Distance off of the centerline	23.2 ft

Given the beam of the ship, it was not possible to fit two pods across the transom and allow them to rotate azimuthally 360 degrees without either extending beyond the sides of the hull or colliding with the other pod while it was also rotating. The pods were placed so that there was no possibility of them colliding, which results in them extending outboard of the ship's beam by as much as 7 ft for some conditions.

The aft propeller is smaller in diameter than the forward propeller to ensure that the entire aft propeller operates in the slipstream of the forward propeller. The ratio between the diameters of the forward and aft propellers will be determined during the parametric study. Typically, the aft propeller's diameter is less than 83% of the forward propeller's diameter.

In the table, a positive shaft angle indicates that the propeller trailing edge is tilted downward; a negative shaft angle indicates that the trailing edge is tilted upward. Figure 7 shows a closer view of one set of contra-rotating propellers. The axis of rotation of each blade row is shown. The axis of rotation of a propeller lies on the propeller's shaft line. In Figure 7 it is visible that the shaft lines of the forward and aft blade rows are not aligned. This is also visible in Table 2 as a 3.9 degree difference in shaft angle between the two blade rows. The forward propeller is angled slightly downward because its motor is housed ahead of it within the hull. The pod is aligned one degree upward at the aft end to align it with the flow over the hull and thereby reduce hull interaction losses. The different shaft angles were not taken into account during the design process; it was assumed that the difference did not greatly affect the steady performance of the contra-rotating set.
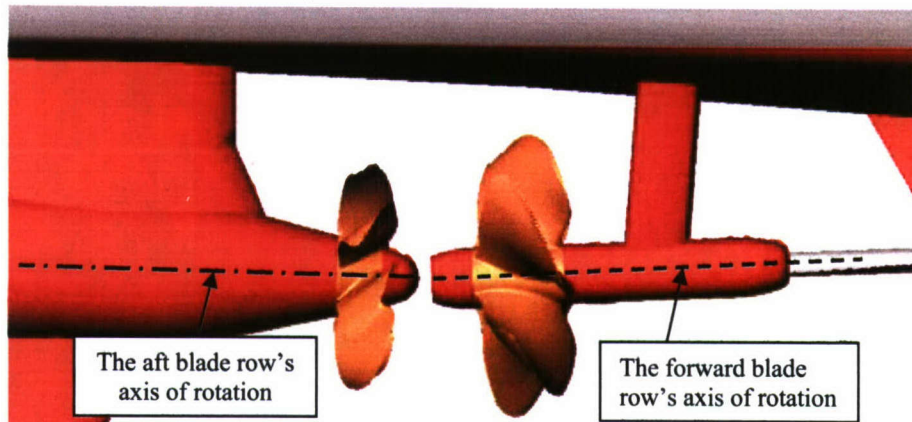
Figure 7. One set of contra-rotating propellers with the axes of rotation shown.

Contra-rotating propellers allow for swirl cancellation. The efficiency of the contra-rotating set can be increased by having finite loading at the root of each propeller. However, finite loading at the root will produce a hub vortex if the swirl is not cancelled. In the above figures, it is visible that there is clearance between the pod fairwater and the tailcone of the forward propeller. It is desirable to minimize the gap between the forward tailcone and pod fairwater because minimizing the gap will minimize the region in which a hub vortex will be present. The forward tailcone is half of a 2:1 ellipse that has been truncated after two-thirds of its length. Although it is not visible in the figures, the aft surface of the tailcone is concave. The radius of the concavity is the azimuth radius of the pod plus three inches because the full scale gap between the pod fairwater and the forward tailcone was originally only three inches. The final gap length is one foot. The gap length was increased to one foot to simplify model scale construction of the HSS Shaft-Pod.

Dual-Pod Configuration

Figure 8 shows a computer generated model of the Dual-Pod configuration (provided by NSWCCD Code 5800[2]). The propeller design for the Dual-Pod configuration will be covered in another report.
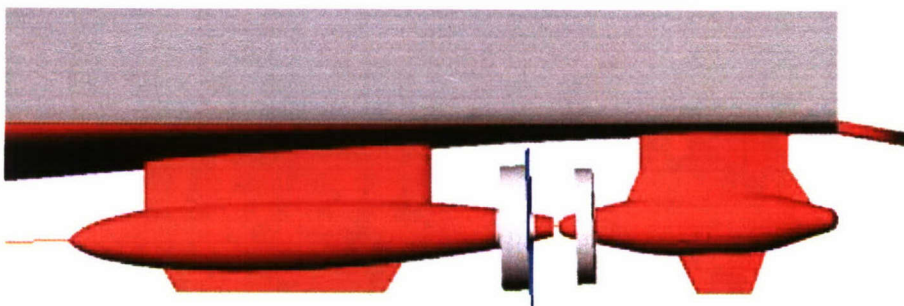
Figure 8. A side view of the Dual-Pod configuration.

REQUIREMENTS

The target speed for the design is 39 knots. Resistance data and calculations were provided by NSWCCD Code 5800[3]. The starboard inboard wake of the model was used as the characteristic wake for the design. The wake survey was measured by NSWCCD Code 5800 [2] on Model 5653-3 in its BSS configuration.

RESISTANCE

The resistance data used for the Shaft-Pod configuration are a combination of Model 5653-3, JHSS BSS model scale test data and calculations to estimate pod resistance. The bare hull and shaft and strut resistance was extracted from the JHSS BSS model scale powering test data [2]. The pod resistance does not include resistance contributions from wave drag. Figure 9 shows the predicted EHP as a function of speed for the Shaft-Pod configuration.
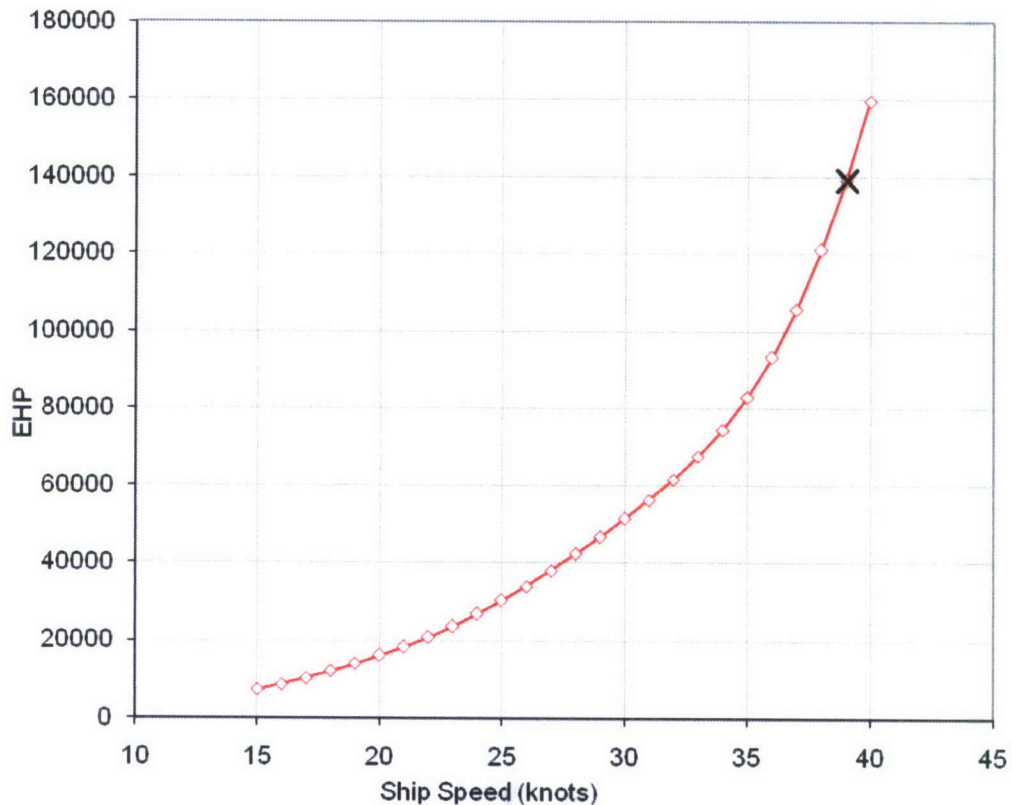
Figure 9. The effective horsepower (EHP) curve for the Shaft-Pod configuration.

---

[3] Email from Jonathan Slutsky to Scott Black on 07/25/2007

A thrust deduction factor, t, of 0.135 was assumed. The thrust deduction factor measured during the four screw powering tests was 0.104 at 39 knots. A larger thrust deduction of 0.135 was chosen to represent this design because there will be interference drag introduced by the azimuthing pods. In past model scale powering tests, pods have given thrust deduction factors ranging from 0.05 to 0.17. Therefore, it was assumed that a thrust deduction factor of 0.135 was a reasonable estimate. To propel this ship at 39 knots with a thrust deduction factor of 0.135, the combined thrust produced by all four propellers must be 1,341,000 lbs.

WAKE SURVEY

Wake data measured on the JHSS BSS, Model 5653-3, were used to estimate the inflow to the forward propeller (the shafted propeller) [2]. The starboard inboard wake was used as the representative wake for this study because the placement of the shafts and struts was similar to the placement of the forward propeller shafts and struts. The inboard wake data was measured with an LDV system at a Froude-scaled full scale ship speed of 36 knots. The wake has a full scale diameter of 21.325 ft (r/R = 1) but contains data out to a diameter of 23.458 ft (r/R = 1.1). The inner diameter of the wake data is 4.265 ft, which corresponds to a non-dimensional radius, r/R, of 0.2. Figure 10 shows the JHSS BSS inboard wake. The wake survey shown in Figure 10 has a nominal wake fraction of 0.127 (1-w = 0.873) for a diameter of 23.458 ft.
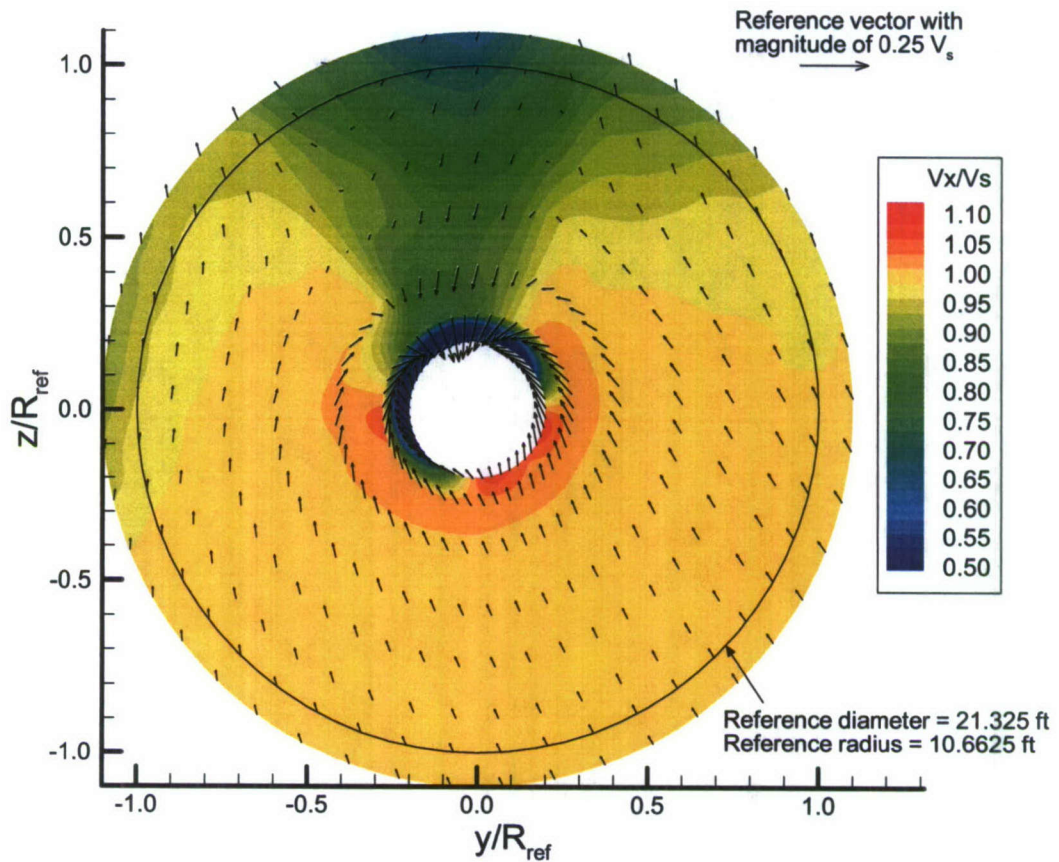
Figure 10. The JHSS BSS inboard starboard wake survey.

In Figure 10 , the two innermost radii of this wake are being affected by LDV measurement error. The large variations in the radial and axial velocities are not representative of the true wake. This error appears because there is no hub present during the wake survey. Without the presence of a hub, the flow is separating when the shaft abruptly ends. The separated flow then begins to move upwards to follow the shape of the hull. As the flow bends behind the shaft, the top of the flow, the separated flow, slows. The bottom part of the flow, the unseparated flow, accelerates.

Corrections were made to the wake to take this known experimental inaccuracy into account. To correct for the errors and make the wake more representative of the assumed Shaft-Pod configuration wake, the two innermost radii of the wake were deleted. To prevent extrapolation, the wake distribution at the non-dimensionalized radius, r/R, of 0.42 was duplicated at a non-dimensionalized radius of 0.2.

Once the above changes to the wake were made, the wake had a nominal wake fraction of 0.0378 (1-w = 0.9622). The wake was scaled to have an effective wake fraction of 0.038 (1-w =

0.962). This wake fraction was taken from the JHSS powering report [2] at 39 knots. Figure 11 shows the resulting wake survey that was used for the forward propeller.
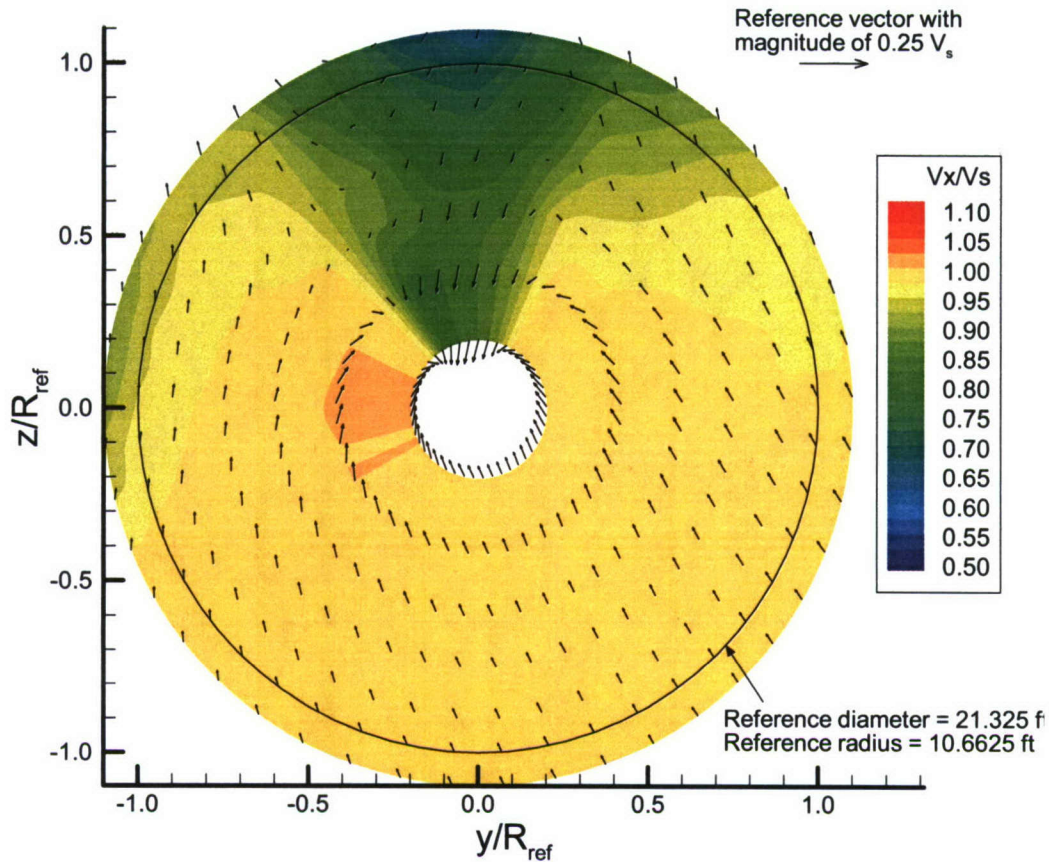
Figure 11. The characteristic wake survey for the forward blade row after modifications.

The wake into the aft blade row was calculated during the parametric study by a lifting line code. The lifting line code calculates the aft wake by first calculating the circumferential mean of the velocities induced by the forward propeller. The mean values of the velocities induced behind the forward propeller are then added to the original forward wake. The resulting wake survey is taken to be the aft wake. The lifting line code also recalculates the forward wake in a similar way. The circumferential mean of the velocities induced by the aft propeller are first calculated. Then, the mean values of the velocities induced ahead of the aft propeller are added to the original wake of the forward propeller. This wake is taken to be the new forward wake.

DESIGN PROCESS

The propulsor design for the Shaft-Pod consisted of two stages. The first stage was the preliminary design and used a lifting line design code [6]. The gross propeller parameters were determined in the preliminary design phase. In this phase, it was assumed that the effect of cavitation on the amount of power required to achieve 39 knots was minimal.

The second stage was the 3D propeller design phase. In this phase, a lifting-surface design code was used to develop blade pitch and camber. The pitch and camber distributions were developed based on the spanwise geometry and loading characteristics developed in the preliminary design stage. The spanwise fairing process was iterated to generate smoothly varying geometry.

PARAMETRIC STUDY

During the parametric study, the values of large scale design variables were chosen. The parametric study tools included a propeller lifting line design code, a cavitation bucket program, and a beam stress program. The propeller lifting line code calculated the forces on each propeller. The cavitation bucket program calculated the cavitation inception speeds and created cavitation bucket plots for each blade row [7]. The maximum stresses on each blade row were calculated by the beam stress program. The output from the parametric study codes included information about thrust, torque, lift coefficients, propeller weight, stress, cavitation, and efficiency.

INITIAL PROPELLER GEOMETRIES

Before the lifting line calculations began, it was necessary to select representative propeller geometry distributions. For this study, the initial geometries for skew, rake, chord, thickness and circulation were taken from the 39 knot high speed propeller design developed for the JHSS BSS (P5506). It was assumed that these were good base geometries because they were intended for a 39 knot propeller on this platform. The initial propeller geometries will be presented later. This contra-rotating set is intended for the starboard side of the ship; the forward propeller is right handed, while the aft propeller is left handed.

DESIGN GOALS

The parametric study aimed to maximize efficiency by minimizing the expanded area ratio, EAR, for each blade row. Lower expanded area ratios translate to less viscous losses on each blade, which results in larger efficiencies. Larger expanded area ratios translate to lower

cavitation inception speeds. Therefore, there is a balance between having a low expanded area ratio that maximizes efficiency and a large expanded area ratio that delays the onset of cavitation.

DESIGN CONSTRAINTS

The design was constrained in the areas of thrust breakdown, cavitation inception speed, hub and blade geometry, lift coefficient, and stress.

Thrust Breakdown

Cavitation is detrimental because it can lead to thrust breakdown, vibration, noise, erosion, and loss of efficiency. A non-cavitating propeller will produce a given amount of thrust at a given RPM. If the propeller is operating at the same RPM but with excessive cavitation, the propeller can lose thrust relative to the non-cavitating condition. This thrust loss is known as thrust breakdown. To overcome thrust breakdown, the propeller's RPM must be increased to recover the lost thrust. Increasing the RPM increases the angle of attack of the blade sections and therefore increases cavitation. At speeds above thrust breakdown inception a large RPM increase might be needed to recover the lost thrust. As the RPM increases, the net increase in thrust can drop until there is no further increase. At that point, the ship has attained absolute top speed and any increase in RPM or power will not increase speed. For some power plants, increasing the RPM is not possible and the thrust loss due to cavitation cannot be recovered. Propellers experiencing thrust breakdown not only lose thrust and efficiency, but can also experience structural damage in the form of erosion or bent trailing edges.

The Burrill chart was developed in the 1940's [8]. At that time, the chart was considered to be the best tool for selecting propeller parameters that would prevent thrust breakdown for single stage propellers. The development of the chart continued through the mid 1960's [9], during which contributions by Gawn [10] were included. Figure 12 shows the Burrill chart, Gawn-Burrill thrust breakdown criteria and SSPA thrust breakdown criteria [11].

Currently, the Burrill chart serves as a rough guide to the likelihood of thrust breakdown. For this design, minimal thrust breakdown was desired at the 39 knot target speed. To ensure minimal thrust breakdown, the blades on both blade rows were constrained to have no more than 10% back cavitation.
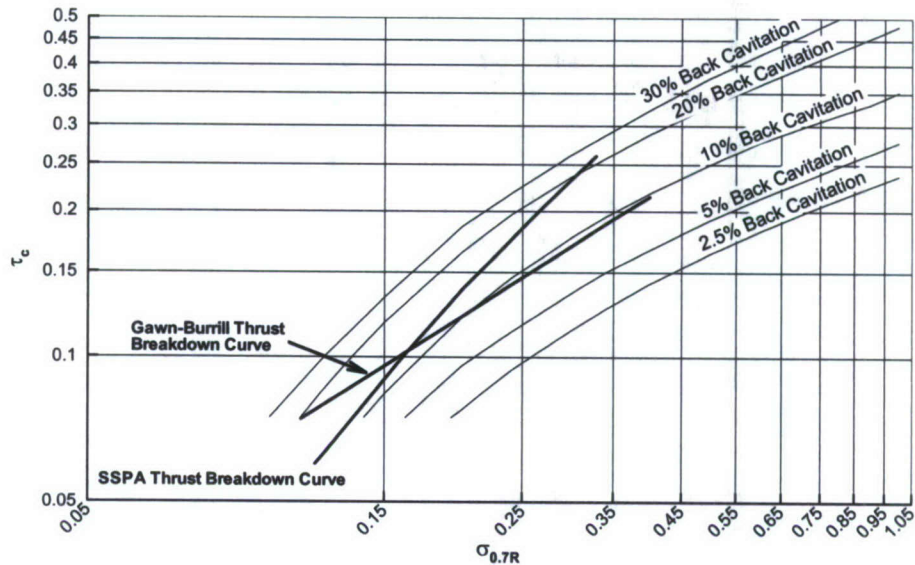
Figure 12. The Burrill chart.

Cavitation Inception

As mentioned above, the Burrill chart is only a rough guide to the likelihood of thrust breakdown. It was desirable to provide another constraint to protect against excessive thrust breakdown at the design speed.

For the 39 knot, high speed design (P5506), special care was taken to minimize thrust breakdown at 39 knots. Because some of the 39 knot design's geometries are being used as a starting point for this design, it was possible to use that design's predicted performance to set a minimum cavitation inception requirement. A 2D cavitation bucket program was used to predict the blade surface cavitation inception speed for each blade row. Preliminary runs during the parametric study suggested that the cavitation inception speed on both blade rows was very low (~14 knots). The final 39 knot high speed design was run with the wake in Figure 11 and it was found that cavitation inception was predicted at 14.5 knots. Therefore, 14.5 knots was used as the minimum cavitation inception speed on both blades rows. By setting a minimum cavitation inception speed, another safety measure was taken to prevent excessive thrust breakdown at the target speed.

Hub and Blade Geometry

The expanded area ratios for both blade rows were constrained to be less than 1.1 for manufacturing simplicity. Blades with a great deal of overlap can be difficult to manufacture.

The forward hub radius was set to be 25% of the forward propeller diameter. The aft hub radius was set to always equal the forward hub radius (and therefore also varied with the forward propeller diameter).

The original intent was to make each propeller's hub length equal to its maximum axial extent. Ensuring that the hub is at least as long as the maximum axial extent ensures that the propeller can be set on either hub face on a flat surface without the blades hitting the surface. Unfortunately, last minute changes to both propeller designs required that the blades of both propellers overhang their hubs on one side. Therefore, when manufactured, both propellers can only be placed on one hub face.

Stress and Lift Coefficient

For both the forward and aft blades, the maximum stress and maximum lift coefficient were constrained to be less than 12,500 psi and 0.4, respectively. Although stress and lift coefficient were constrained, neither violated their bounds during the parametric study.

DESIGN VARIABLES

Table 3 shows the design variables and their associated ranges.

Table 3. The parametric study design variables and associated ranges.

Design Variable	Lower bound	Upper Bound
D_1	20 ft	23 ft
D_{ratio} (D_2/D_1)	0.71	0.83
RPM_1	80	200
RPM_{ratio} (RPM_2/RPM_1)	0.5	1.5
P_{ratio} (P_2/P_1)	0.5	0.6
Z_1	5 or 7 blades	
Z_2	7 or 5 blades	

The upper bound of the forward propeller diameter was constrained by the geometry of the Shaft-Pod arrangement. A forward propeller diameter of 23 ft keeps the propeller above the baseline of the ship and allows for a propeller tip clearance of 20%. A smaller tip clearance was not an option for this design; excessive hull vibrations would most likely occur at high speeds due to cavitation induced pressure pulses.

The diameter ratio, D_{ratio}, is the ratio of the aft propeller diameter to the forward propeller diameter $(D_{ratio} = D_2/D_1)$. The upper bound of the diameter ratio was set equal to the propeller slipstream contraction ratio. Constraining the diameter ratio to be below 0.83 ensures that the aft propeller will always be operating entirely in the slipstream of the forward propeller.

The RPM of the forward propeller was given a large range because it is a shaft and strut mounted propeller. The RPM ratio, RPM_{ratio}, design variable is the ratio of the negative aft

propeller RPM to the forward propeller RPM $\left(RPM_{ratio} = -RPM_2/RPM_1\right)$. Power ranges and the associated RPMs of different Azipod models were provided in the ABB Azipod Guide [3]. Figure 13 shows a plot of power ranges and RPMs for differently sized Azipods. The 'Type 28' pod motor is the 25 MW pod being used for this design. Although the 'Type 32' unit is on the chart and has more power, it was not an option for this design because it is still in development. Although the figure suggests that at 25 MW, the RPM must be between approximately 110 and 125, correspondence with ABB revealed that the motors can be made to operate efficiently over a wider range of RPMs. Therefore, the RPM ratio was given a large range.

The power ratio is equal to the ratio of the aft power to the forward power $\left(P_{ratio} = P_2/P_1\right)$. The main role of the power ratio in the parametric study was to determine how much power the forward propeller needed to achieve a ship speed of 39 knots.

The number of blades on the forward and aft blade rows was five and seven or seven and five, respectively. These blade numbers were chosen to reduce unsteady forces. Because manufacturing simplicity was desired, larger numbers of blades were not considered. Additional inputs into the lifting line program are detailed in Appendix A.
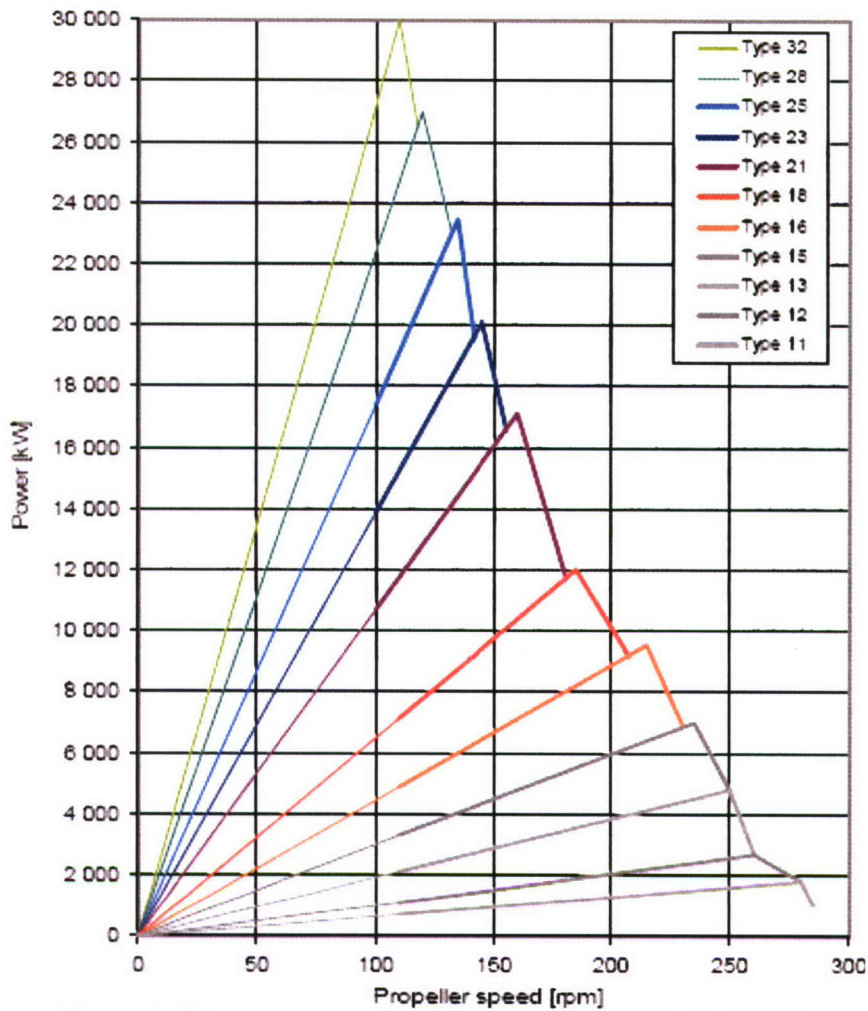
Figure 13. The power ranges and RPMs of different Azipod units [3].

RESULTS OF THE PARAMETRIC STUDY

Systematic calculations were performed with the parametric study tools for discrete values of the parameters in Table 3 over the ranges shown. Once the performance of all desired design variable combinations was calculated, simple scatter plots were used to identify trends within the results.

Figure 14 shows a sample results plot. This plot shows all of the design points that satisfied all of the constraints for design variable combinations with a diameter ratio of 0.77.
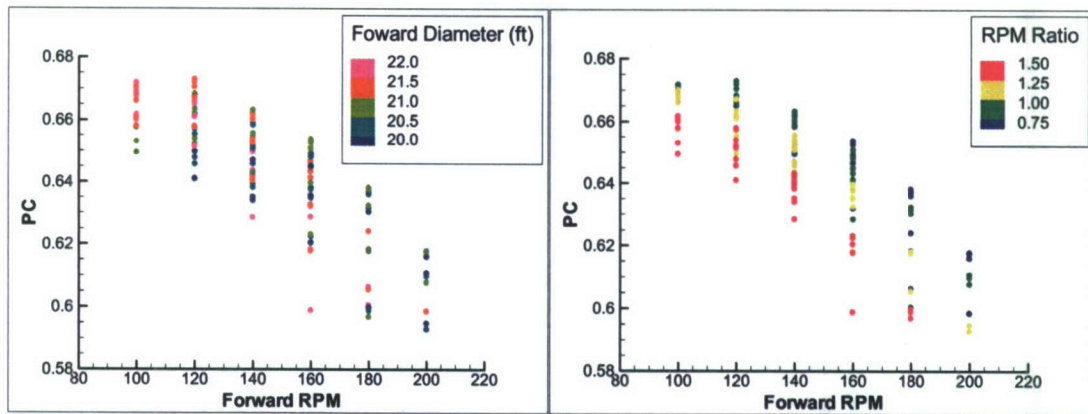
Figure 14. Sample parametric study results for design variable combinations with a diameter ratio of 0.77.

Figure 14 shows how the propulsive coefficient varied with the forward propeller RPM and diameter and how the propulsive coefficient varied with the forward propeller RPM and the RPM ratio. These plots helped to show trends within the results. For example, at the diameter ratio shown in Figure 14, larger forward diameters gave larger efficiencies. Efficiency increased as the RPM ratio decreased and peaked at a forward RPM of 120 RPM. Also, very few design points with an RPM ratio of 0.75 met the percent back cavitation, expanded area ratio and cavitation inception speed constraints.

After generating many plots like Figure 14 and continuously narrowing the design space, a nominal design point was chosen. The point that was chosen gave the best combination of maximum efficiency, maximum cavitation inception speed, and minimum expanded area ratio. Since the optimum RPM ratio was approximately one, an RPM ratio of one was chosen to simplify gearing during model scale tests. An RPM ratio of one could also provide a commonality in the motors if electric motors were used to drive the forward propellers. A power ratio of 0.5 was chosen because the forward blade row needed 50 MW to augment the 25 MW in the pod and achieve 39 knots. With 150 MW (201,150 hp) provided by the motors, a propulsive coefficient of at least 0.69 was needed to achieve 39 knots. If it had been possible to achieve a propulsive coefficient above 0.69, it would have been possible to use a smaller motor and therefore have a smaller pod. A smaller pod would have improved the overall hydrodynamic performance of the HSS Shaft-Pod.

Table 4 shows the design variables of the nominal design point and some performance characteristics.

Table 4. The nominal design point after the first stage of the parametric study.

Variable	Nominal Value
D_2/D_1	0.79
RPM_2/RPM_1	1.00
P_2/P_1	0.5
PC	0.676

Variable	Nominal Value (Forward Blade Row)	Nominal Value (Aft Blade Row)
Diameter	21.5 ft	17 ft
RPM	113	-113
EAR	0.926	0.873
Cavitation Inception Speed	14.7 knots	19.2 knots
C_L	0.29	0.26
Stress	4800 psi	6200 psi
Percent Back Cavitation	10	10

DESIGN OPTIMIZATION

Once the nominal design point was chosen, the forward and aft circulation distributions were optimized. The lifting line code can calculate the optimum circulation given chord, inflow, thickness, number of blades, thrust, diameter and RPM. Optimizing the circulation will generally give a better propulsive efficiency at the expense of cavitation inception speed. Often, in order to meet other criteria, the circulation distribution will become a compromise between the optimal circulation and the one that satisfies performance requirements.

Figure 15 shows a plot of the original and optimal circulation distributions. The solid lines represent circulation distributions for the forward propeller while the dotted lines show the corresponding aft circulation distributions. Although the aft blade row has negative circulation, the distributions are plotted as positive here to show the relative magnitudes between the forward and aft circulations.
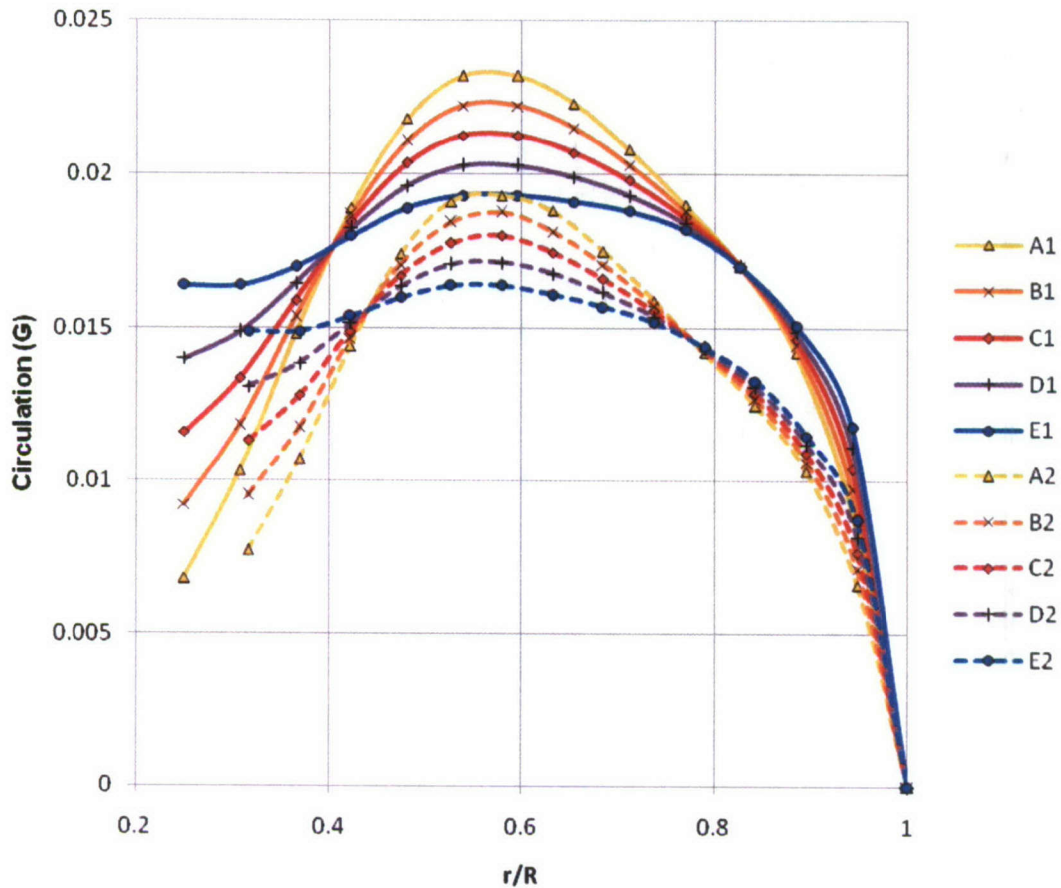
Figure 15. The initial and optimal circulation distributions and the circulation distribution compromises.

The optimum circulation distribution for both blade rows (E1 and E2) had less loading near the middle radii and larger loading at the root than the original distributions (A1 and A2). The optimum circulation distribution increased the propulsive coefficient to 0.694 (a two point increase in efficiency), but dropped the cavitation inception speed on the aft blade row by three knots. The cavitation inception speed on the forward blade row did not change significantly.

In order to take advantage of some of the efficiency increase while still maximizing the cavitation inception speed, the performance of three different interpolations of the original and optimal circulation distributions were calculated. The three combinations are shown in Figure 15. In the figure, the 'B1' and 'B2' distributions are similar to the original distribution, but with some of the characteristics of the optimal distribution. The 'D1' and 'D2' distributions, however, are closer to the optimal distribution with a few characteristics of the original distribution.

The performance of all three interpolated circulation distribution sets was calculated. Table 5 shows the performance of the initial, optimum and three interpolated circulation distribution sets with respect to the propulsive coefficient and the cavitation inception speed on

both blade rows. For all three distributions, both the forward and aft blade rows had 10% back cavitation. The 'D' circulation distributions were chosen for this design. The 'D' distributions gave the best propulsive coefficient and the largest cavitation inception speeds for both blade rows.

Table 5. The performance of the initial, optimum and interpolated circulation distributions.

Circulation Distributions	PC	Forward Cavitation Inception Speed (knots)	Aft Cavitation Inception Speed (knots)
A	0.676	14.7	19.2
B	0.682	15.1	17.8
C	0.686	15.2	16.8
D	0.686	16.0	19.4
E	0.694	14.8	16.6

Once the circulation distributions were chosen, fair chord and thickness distributions were developed. Figure 16 shows the resulting lift coefficient distributions. Table 6 shows the resulting propulsive coefficient and cavitation inception speeds. Figure 17 shows the initial and modified chord distributions. Figure 18 shows the initial and modified thickness distributions.
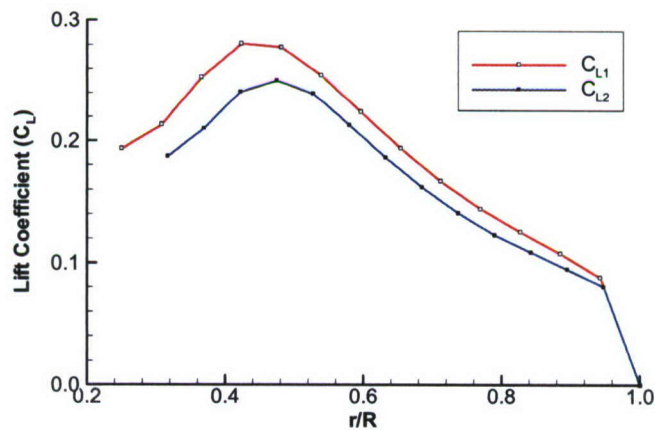
Figure 16. The lift coefficient distributions after changes to the chord, thickness, and circulation distributions.

Table 6. The propulsive coefficient and cavitation speeds after the lift coefficients were smoothed.

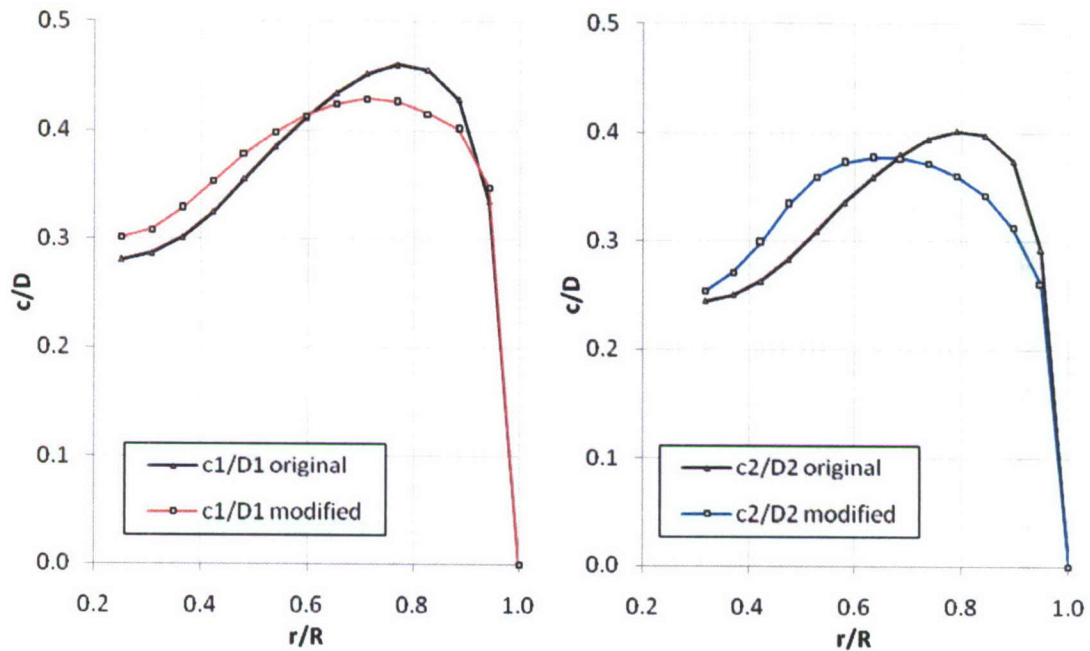| Circulation Distributions	PC	Forward Cavitation Inception Speed (knots)	Aft Cavitation Inception Speed (knots)
D – before lift coefficient smoothing	0.686	16.0	19.4
D – after lift coefficient smoothing	0.686	16.2	19.1

Figure 17. The initial and modified chord distributions.
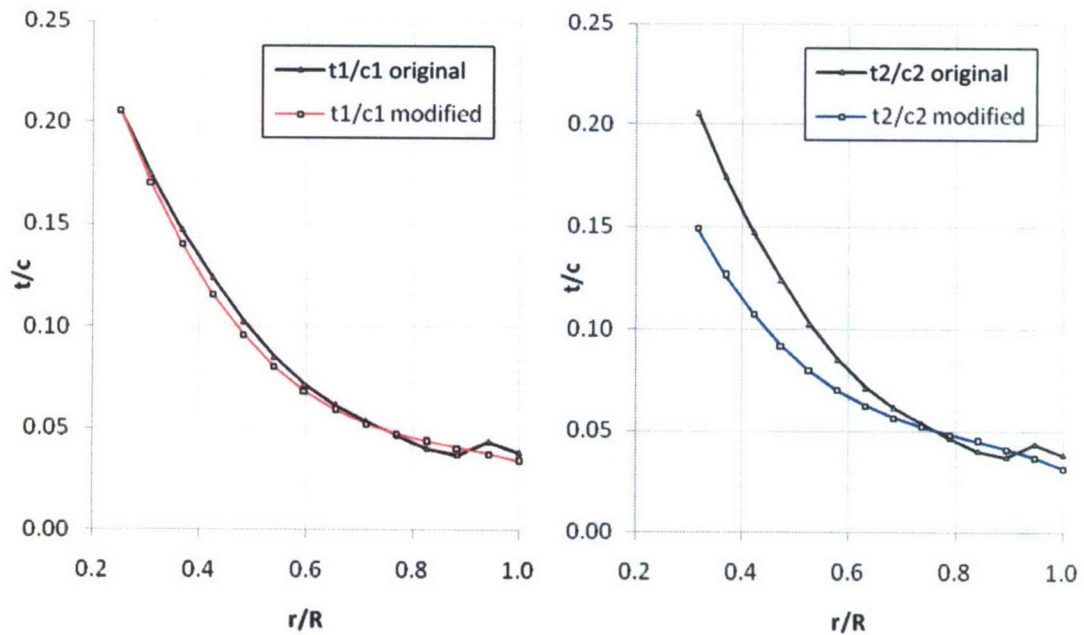

Figure 18. The initial and modified thickness distributions.

A notional skew based on the 39 knot design was used for this design. Unsteady forces were not assessed in this study. The skew of the aft blade row is simply the negative of the forward blade row skew. The rake and skew distributions were not varied during the parametric study. The rake and skew distributions are shown in Figures 19 and 20.
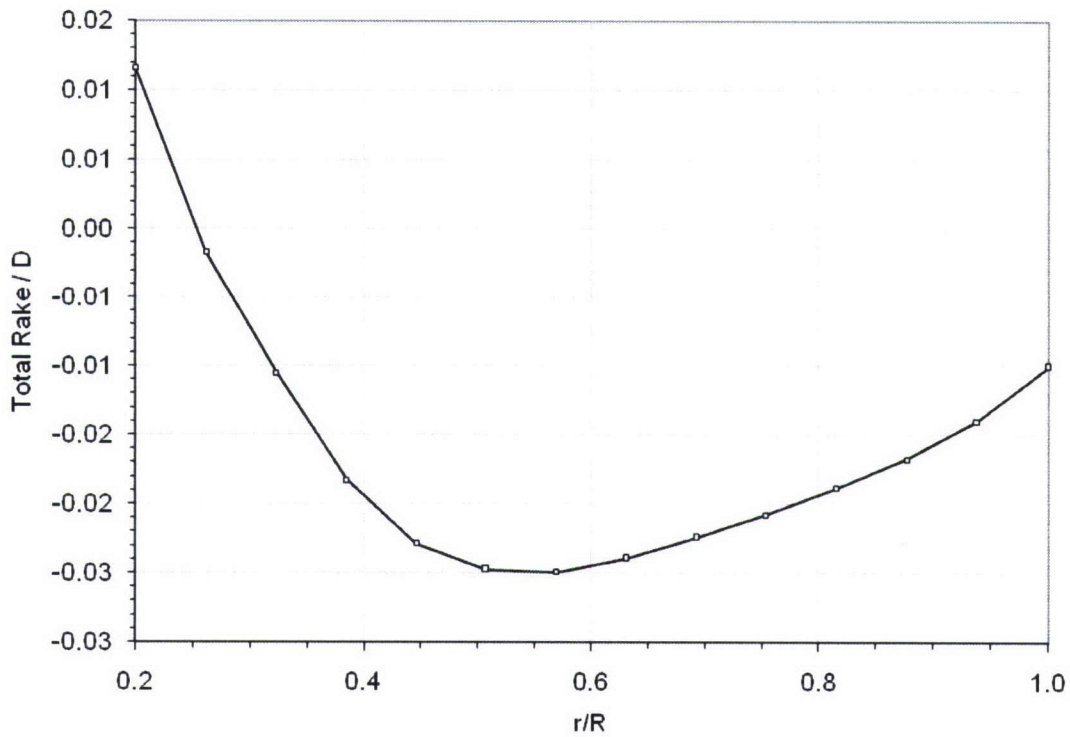
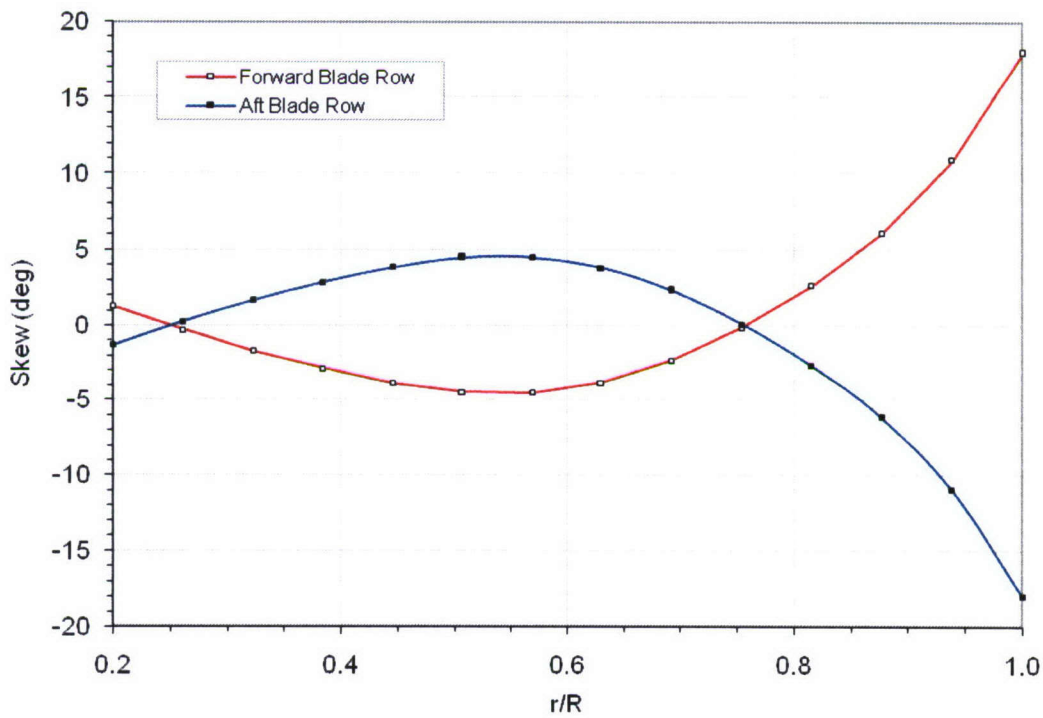**Figure 19. The rake distribution for both blade rows.**

Figure 20. The skew distribution for the forward and aft blade rows.

DESIGN POINT

Table 7 displays the particulars of the final lifting line design point. These values were used as the initial inputs to the 3D lifting surface code.

Table 7. The design point at the conclusion of the parametric study.

Variable	Value
D_2/D_1	0.79
RPM_2/RPM_1	1.00
P_2/P_1	0.5
PC	0.686

Variable	Value (Forward Blade Row)	Value (Aft Blade Row)
Diameter	21.5 ft	17 ft
RPM	113	-113
EAR	0.953	0.895
Cavitation Inception Speed	16.2 knots	19.1 knots
C_L	0.27	0.23
Maximum Principal Stress	4000 psi	9000 psi
Percent Back Cavitation	10	10

Figure 21 shows the Burrill chart that was discussed in the Thrust Breakdown section. The locations of the forward and aft propellers for the HSS Shaft-Pod are shown on the chart. It can be seen that both propellers will experience approximately 10% back cavitation at the full power condition.
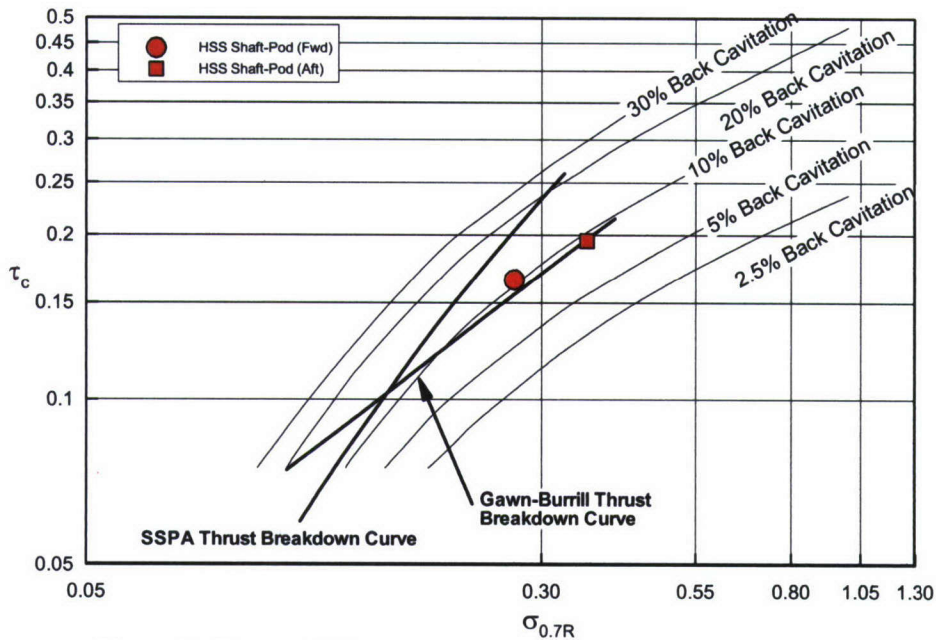
Figure 21. The two HSS propeller designs shown on the Burrill chart.

DETAILED DESIGN

The pitch and camber distributions were determined during the detailed design stage. The open water curves and powering performance were then computed using an analysis of the final blade geometries.

PITCH AND CAMBER DISTRIBUTIONS

During this stage of the design, the forward and aft blade shapes that produced the desired circulation distributions were iteratively calculated. The pitch and camber distributions were determined using a lifting surface design code, PBD14 [12], coupled with an axisymmetric flow solver, MTFLOW [12]. Figure 22 shows the relationships between the design codes used during this stage of the design process.
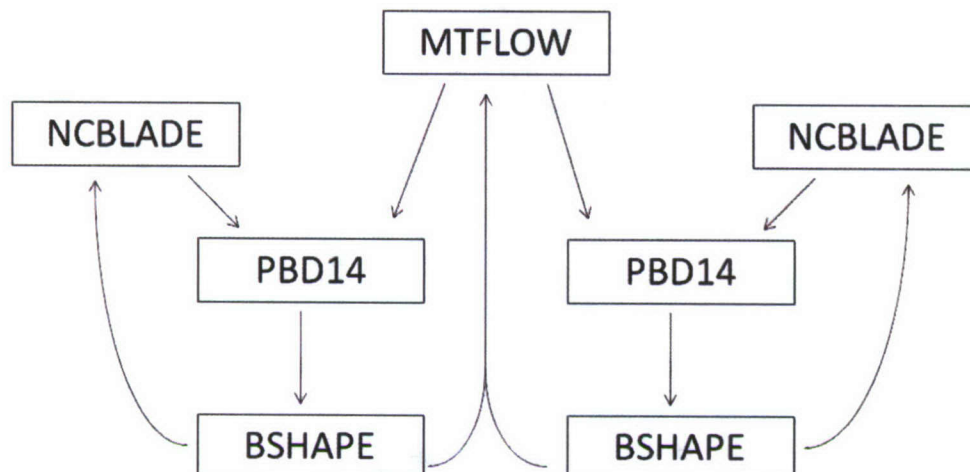
Figure 22. A flowchart showing the relationships between the codes used during the detail design.

First, the axisymmetric hub and casing geometry was defined in MTFLOW. The code read the geometry in as a table of points and fit the points with a cubic spline. A grid was generated according to a set of prompted user inputs. The grid was defined such that there would be adequate resolution in the region of the blade and its wake. The geometry domain was solved and an output velocity file was generated for use as input to PBD14.

The second input to PBD14 was a B-spline net defining the mean camber surface of the blade. This was generated by NCBLADE. NCBLADE is a propeller blade geometry program capable of using spanwise parameter inputs to generate blade geometry in Cartesian coordinates. The initial spanwise parameters were generated by the lifting line code during the parametric study. This process was run independently for each blade row.

PBD14 is a vortex-lattice code capable of designing and analyzing propeller geometry. The PBD14 input files contain information on the velocity field, blade shape, and desired circulation distribution. The code was executed independently for each blade row. PBD14 outputs the blade forces and velocities at the control points. These induced velocities are passed back to the flow solver MTFLOW to define the blade's impact on the flow field.

These velocities are also used by the program BSHAPE to shape the blade such that the incremental mean line slope of the pitch and camber distributions are given by:

$$\delta = \frac{V_n}{V_c} \tag{1}$$

The program BSHAPE is also run independently for each blade. In Equation 1, V_n is the velocity normal to the surface and V_c is the velocity tangent to the surface in the chordwise direction. The BSHAPE program outputs new pitch and camber distributions which were passed to NCBLADE for use on the next iteration. The iterative shaping of the blade, and solving of the flow field continued until the normal component of velocity at the blade surface was zero.

Once the pitch and camber distributions had been calculated, they were faired to give smoother blade shapes. Splines and polynomials were used to fair the distributions. Figure 23 shows the faired pitch distribution for the forward blade row.
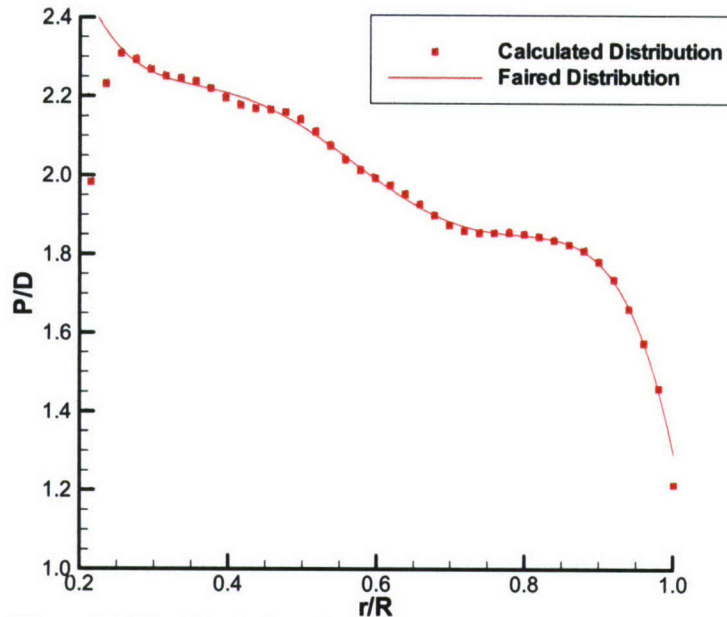

Figure 23. The faired pitch distribution for the forward blade row.

This pitch distribution was faired using a high order polynomial. The first and last points of the distribution were ignored during the fairing process. The chordwise camber was faired using a spline that was fit to a reduced number of points.

The trailing edge radius was increased to allow for a minimum radius of 0.0033 inches (1 mm) model scale to simplify fabrication of the blades. Because the trailing edge radius was increased for robustness during model scale manufacturing, trailing edge details were not included.

 The fillets created on both blade rows had a radius of one-third of the local thickness (T/3). The minimum fillet radius was set to be 0.03 inches model scale.

The forward blade row was defined using cylindrical geometry. However, the conical aft hub (due to the pod shape) made it necessary to define the aft blade row using a cone angle. The cone had an angle of approximately 13 degrees, with the cone diameter increasing aft. This cone angle varied linearly from root to tip with the cone angle reaching zero degrees at the tip [13].

FINAL GEOMETRIES

Figure 24 shows 3D views of one blade of the forward propeller. Figure 25 shows the final forward geometry distributions. Figure 26 presents the blade section views of the forward blade row in full scale units.
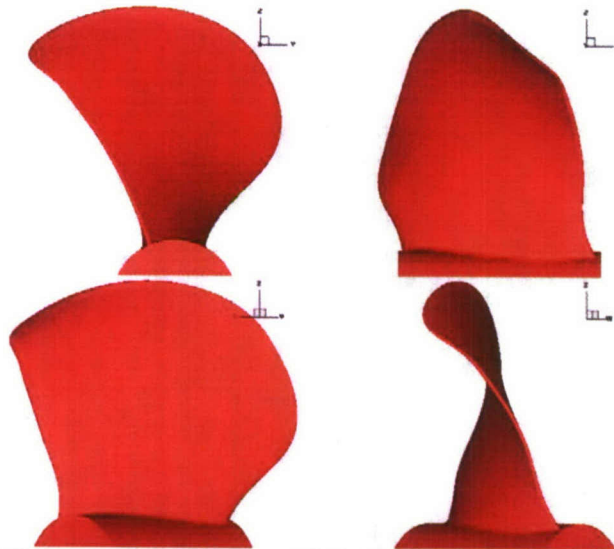

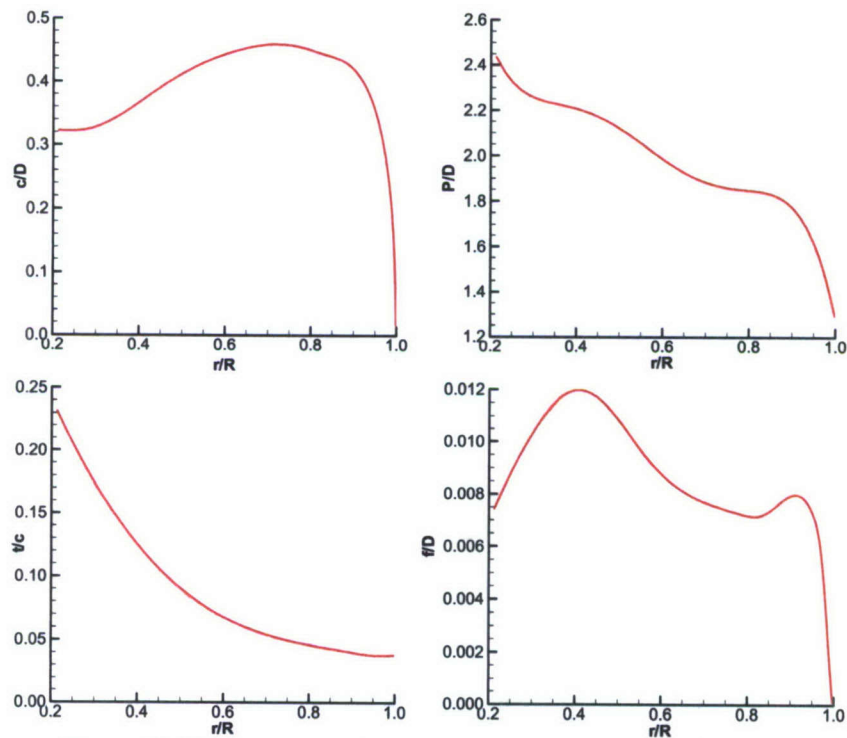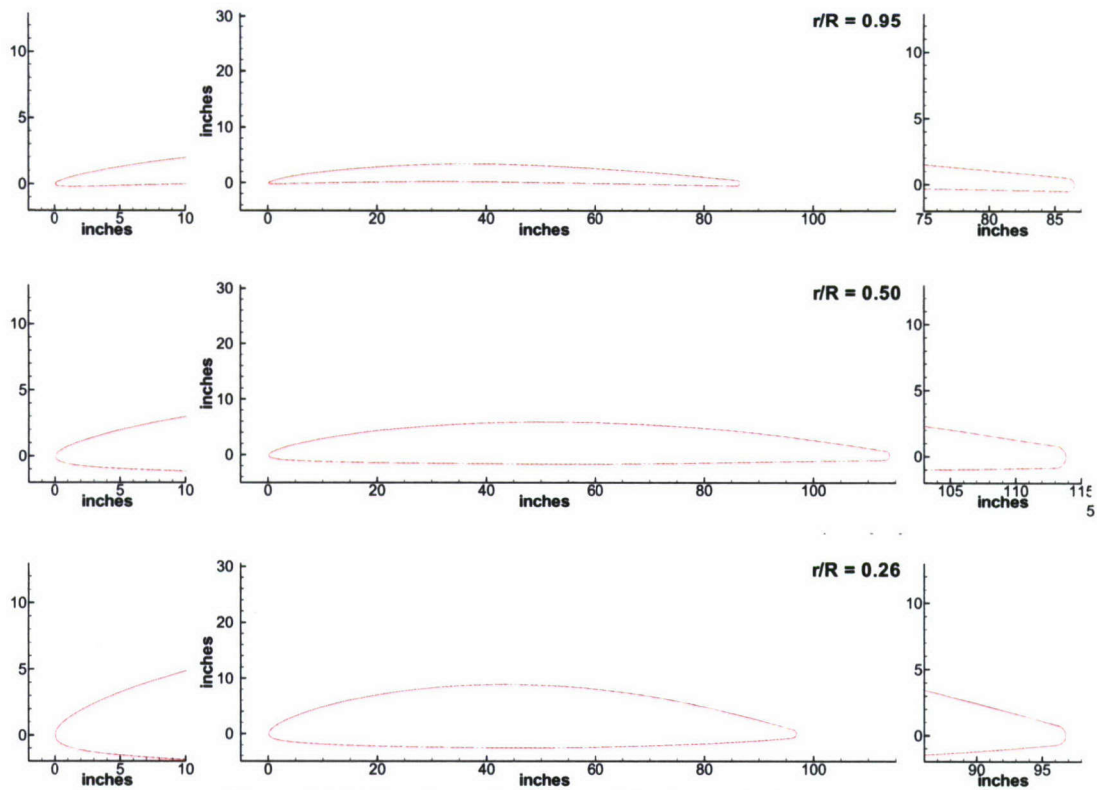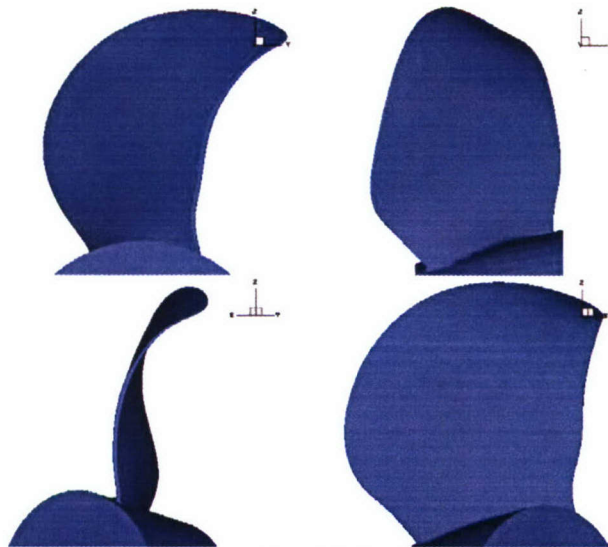**Figure 24. 3D views of one blade of the forward propeller.**

Figure 25. Final geometry distributions for the forward blade row.

Figure 26. Full scale section views of the forward blade row.

Figure 27 shows 3D views of one blade of the aft propeller. Figure 28 shows the final aft geometry distributions. Figure 29 presents the full scale section views of the aft blade row.

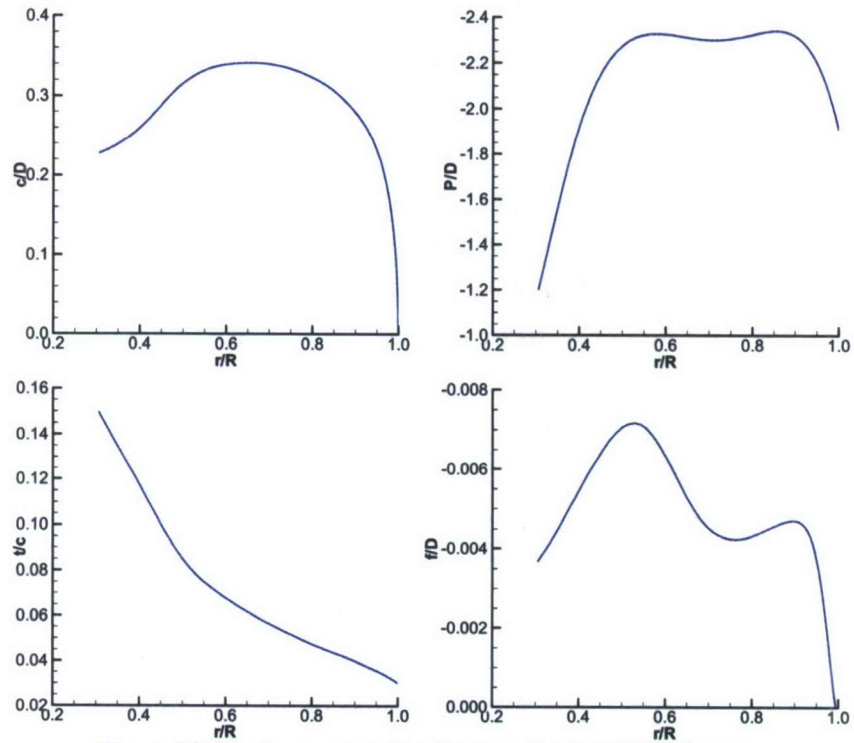**Figure 27. 3D views of one blade of the aft propeller.**

Figure 28. Final geometry distributions for the aft blade row.
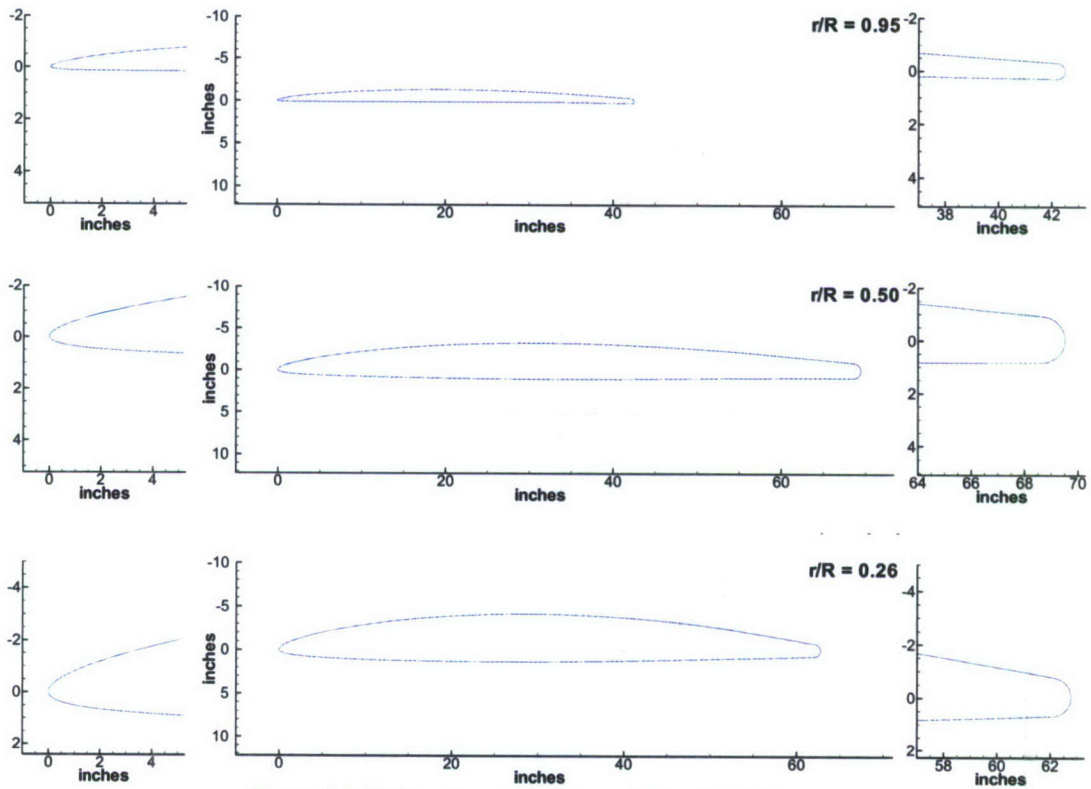

Figure 29. Full scale section views of the aft blade row.

These propellers are currently being manufactured at model scale for testing. The forward propeller numbers are P5513 and P5514 (starboard and port), while the aft propeller numbers are P5515 (starboard and port). The propeller drawings are shown in Appendix B.

A total of eight propellers are being made. All eight propellers are being made using SLA. Four of the propellers (one RH forward propeller, one LH forward propeller, one RH aft propeller, one LH aft propeller) will be coated with epoxy paint. The other four propellers (one RH forward propeller, one LH forward propeller, one RH aft propeller, one LH aft propeller) will be sprayed with a metal coating to increase structural strength.

OPEN WATER AND POWERING CURVES

Performance predictions were made using MTPBD in analysis mode at the design points. The torque and thrust coefficients of the unfaired and faired geometries were compared against the values estimated during the parametric study. Table 8 shows this comparison. In Table 8, it is visible that the fairing did slightly alter the thrust and torque coefficients. The most notable change was in the thrust coefficient of the aft blade row. Fairing the aft blade increased the thrust coefficient by approximately 0.06.

Table 8. The open water torque and thrust analysis.

	Coefficient	Parametric Study	Unfaired at design J=1.572	Faired
Forward Blade Row	K_T	0.2872	0.2815	0.2801
	K_Q	0.0967	0.0919	0.0916
	η	0.743	0.766	0.765
Aft Blade Row	K_T	0.4044	0.4061	0.4607
	K_Q	0.1569	0.1556	0.1704
	η	0.645	0.653	0.677

The open water curves were computed in MTPBD with an RPM ratio of one. Figure 30 shows the combined open water curves for the forward and aft blade rows. The blade rows have a combined advance ratio, J, of 1.572. This advance ratio corresponds to an open water efficiency of 80%, a thrust coefficient of 0.46, and a torque coefficient of 0.14. The thrust and torque coefficients were defined by normalizing the thrust and torque produced by each blade row by the forward propeller diameter and RPM and then adding the values from each blade row together.
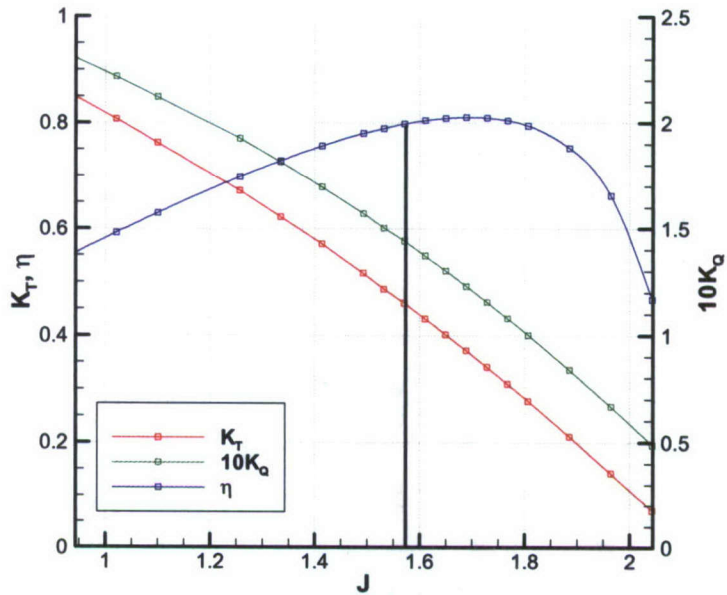
Figure 30. The combined open water curves.

A powering analysis was performed in POWER using the open water calculations and JHSS BSS resistance data. In Figure 31, the RPM and propulsive coefficient $\left(PC = \dfrac{EHP}{DHP} \right)$ are plotted over a range of operating speeds. The results show that a propulsive coefficient of approximately 0.716 and an RPM of 111 are expected at the 39 knot design speed. Table 9 shows a comparison of the predicted powering performance to the JHSS BSS hull form powering data.
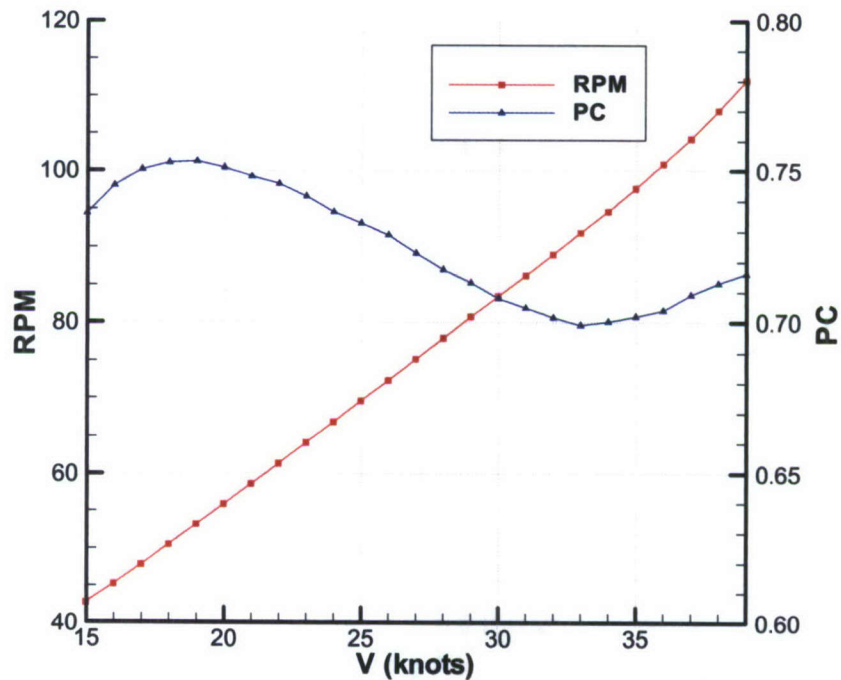

Figure 31. The combined powering curve.

Table 9. A comparison of the HSS Shaft-Pod powering calculations to the JHSS BSS powering data.

	Speed (knots)	EHP (hp)	DHP (hp)	PC
Design (Shaft-Pod)	39	138900	191500	0.725
Stock Powering (BSS)	39	148000	231300	0.640
% Difference		-6.15%	-17.2%	13.3%

CONCLUSIONS

The final contra-rotating design has a 21.5 foot diameter, five-bladed propeller forward and a 17 foot diameter, seven-bladed propeller aft. Both the forward and aft propellers operate at 113 RPM. Calculations predict that the design will achieve the 39 knot target speed without significant thrust breakdown. A final propulsive coefficient of 0.716 is predicted at 39 knots with 191,500 DHP. A propulsive coefficient of 0.64 was measured for the JHSS with four shafts and struts with 213,300 DHP. Therefore, this design predicts a 17% decrease in the required DHP.

Open water tests are scheduled for December 2007. Powering tests are scheduled for January 2008. During the open water tests, all four sets of contra-rotating propellers will be tested. The open water curves of the contra-rotating set will be determined during these tests. The open water tests will also be used to evaluate the performance of the propellers with the metal coating against the performance of the propellers with the epoxy paint.

ACKNOWLEDGEMENTS

APPENDIX A – PARAMETRIC STUDY INPUTS

Table A-1 displays the inputs into the lifting line code.

Table A-1. The inputs to the propeller lifting line code.

Variable	Input Value
Shaft Depth	17.5 ft
Axial Spacing	11 ft
Non-Dimensional Forward Hub Radius	0.25
Dimensional Aft Hub Radius	Forward Hub Radius (ft)
Forward Wake Diameter	21.325 ft
Aft Wake Diameter	17.7 ft

In the table, the shaft depth is taken to be at the centerline of the forward blade row. The axial spacing is measured from the centerline of the forward blade row to the centerline of the aft blade row. The forward hub radius is non-dimensionalized by the radius of the forward blade row. The aft hub radius is equal to the dimensional value of the forward hub radius. The forward wake diameter is the wake diameter from the wake survey. Finally, the aft wake diameter is the forward wake diameter scaled down by 0.83, the slipstream contraction ratio.

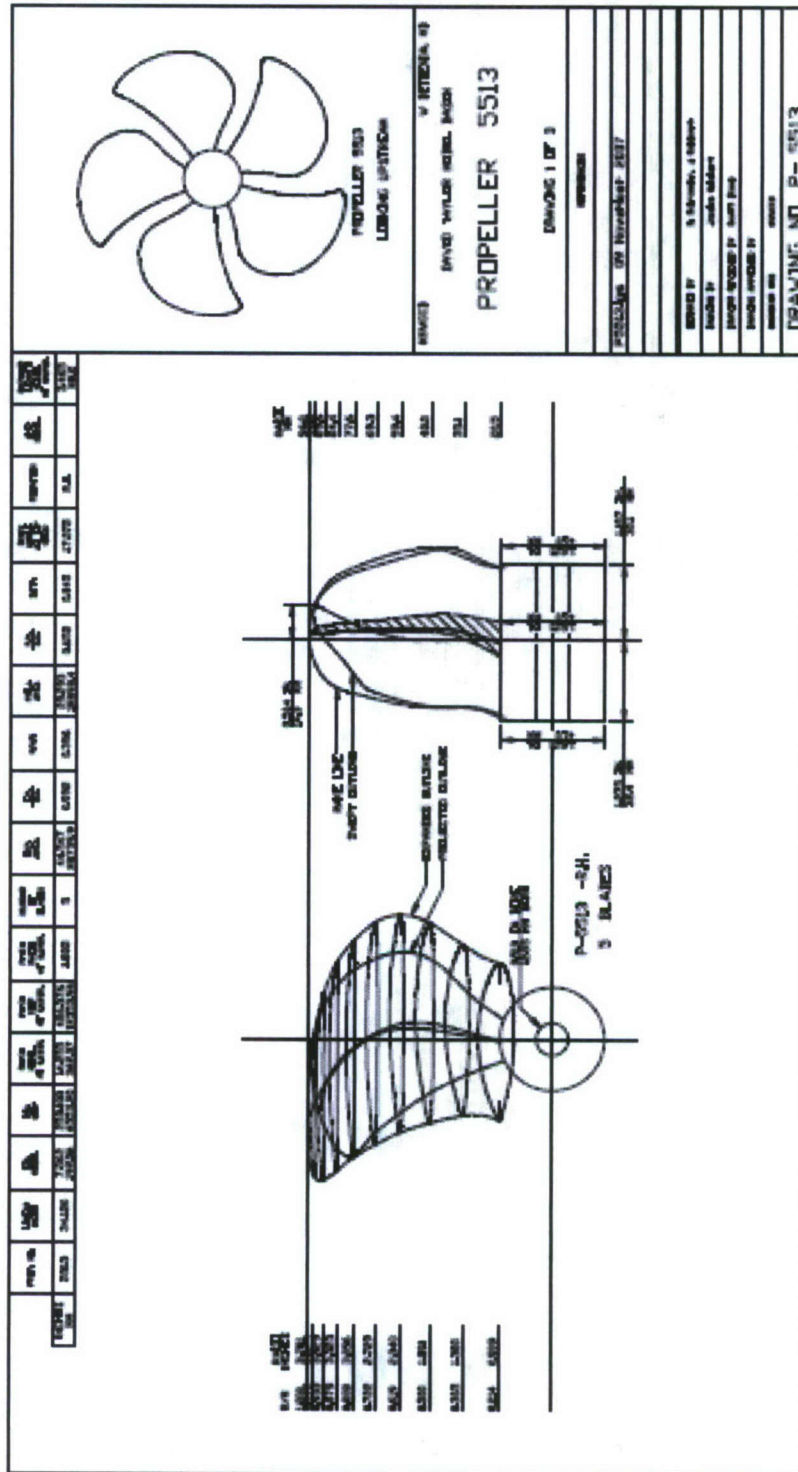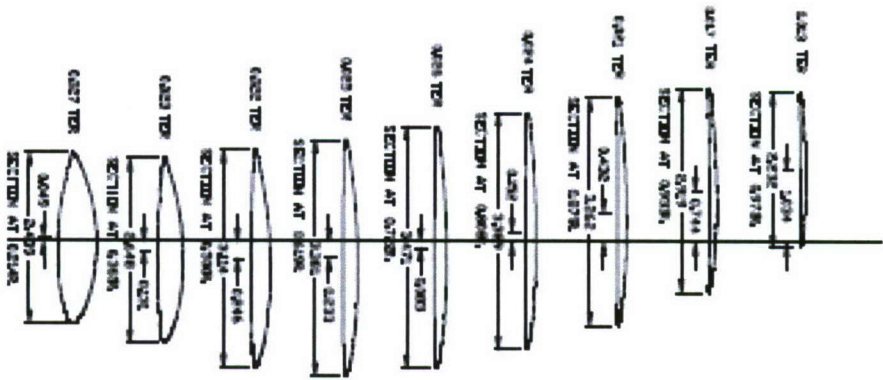**(THIS PAGE INTENTIONALLY LEFT BLANK)**

Figure B-1. The propeller drawing for Propeller 5513 (Drawing 1 of 2).

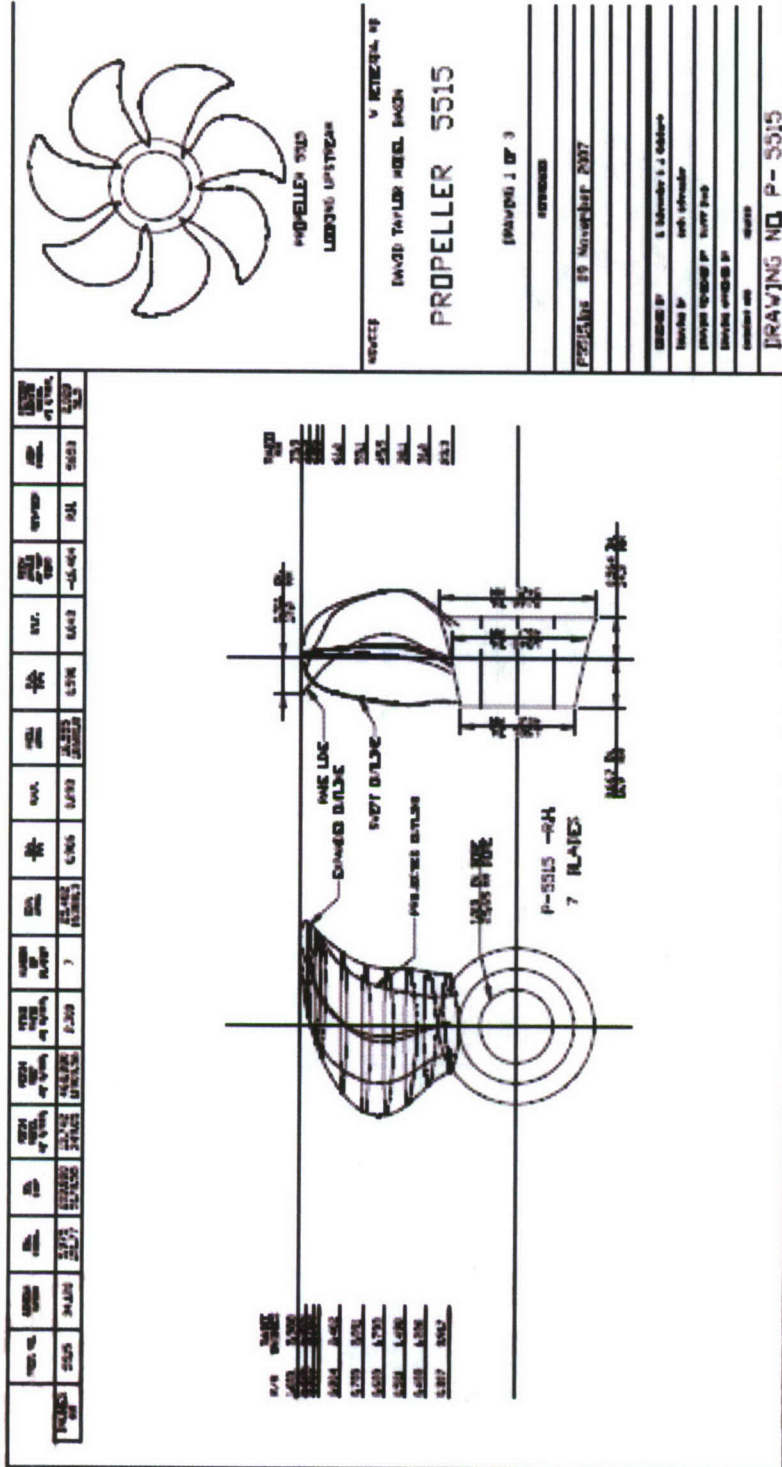Figure B-2. The propeller drawing for Propeller 5513 (Drawing 2 of 2).

Figure B-3. The propeller drawing for Propeller 5515 (Drawing 1 of 2).
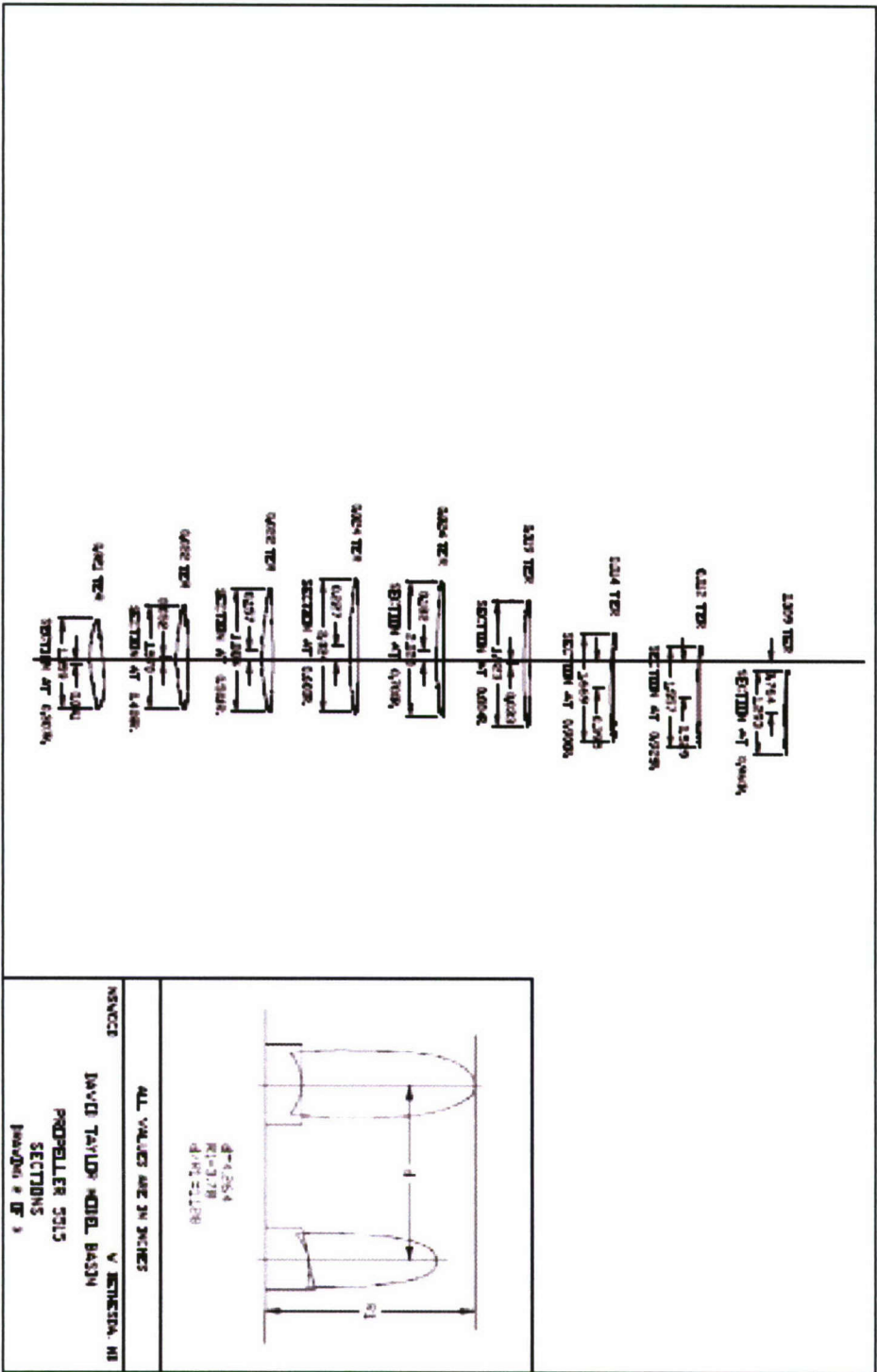
Figure B-4. The propeller drawing for Propeller 5515 (Drawing 2 of 2).

REFERENCES

1. Cusanelli, D. S., Carpenter, S., Powers, A. M., "Axial Waterjet (AxWJ) Model 5662 and Mixed-Flow Waterjet (MxWJ) Model 5662-1: Comparisons of Hull Resistance and Model-Scale Powering with Propulsion Nozzle Designs", NSWCCD-50-TR-2007/076 (November 2007).

2. Cusanelli, D. S., Chesnakas, C. J., "Joint High Speed Sealift (JHSS) Baseline Shaft & Strut (BSS) Model-5653-3: Series 2, Propeller Disk LDV Wake Survey; and Series 3, Stock Propeller Powering and Stern Flap Evaluation Experiments," NSWCCD-50-TR-2007/007 (March 2007).

3. *Project Guide for Azipod® Propulsion Systems, Version 4.1.0*, ABB Marine & Turbocharging (January 2004).

4. "Breakthrough for CRP Azipod," MarineLog.com Article (April 17, 2003).

5. Cusanelli, D. S., "Joint High Speed Sealift (JHSS) Baseline Shaft & Strut (Model 5653) Series 1: Bare Hull Resistance, Appended Resistance, and Alternative Bow Evaluations," NSWCCD-50-TR-2007/066 (August 2007).

6. Coney, W. B., "A Method for the Design of a Class of Optimum Marine Propulsors," MIT D-0-G-4 Doctoral Dissertation (August 1989).

7. Brockett, T. E., "Minimum Pressure Envelopes for Modified NACA-66 Sections with NACA a=0.8 Camber and Buships Type I and Type II Sections," DTNSRDC Report 1780 (February 1966).

8. Burrill, L. C., "Developments in Propeller Design and Manufacture for Merchant Ships," *Transactions*, Institute of Marine Engineers, London, Vol. 55 (1943).

9. Burrill, L. C. and A. Emerson, "Powering Cavitation: Further Tests on 16-Inch Propeller Models in the King's College Cavitation Tunnel," Transactions of the North East Coast Institution of Engineers and Shipbuilders, Vol. 78, pp. 295-320 (1963-64).

10. Gawn, R. W. and L. C. Burrill, "Effect of Cavitation on the Performance of a Series of 16 inch Model Propellers," R.I.N.A. Transactions (1957).

11. Rutgersson, O., "Cavitation on High Speed Propellers in Oblique Flow-Influence of Propeller Design and Interaction with Ship Hull," 13th Symposium on Naval Hydrodynamics, Tokyo, Japan (October 1980).

12. Kerwin, J.E., T.J. Michael, and S.K. Neely, "Improved Algorithms for the Design/Analysis of Multi-Component Complex Propulsors," SNAME Propeller and Shafting Symposium (2006).

13. Neely, S.K., "Non-Cylindrical Blade Geometry Definition," SNAME Propeller and Shafting Symposium (1997).

(THIS PAGE INTENTIONALLY LEFT BLANK)

INITIAL DISTRIBUTION

Number of copies			
Print	**PDF**	**Office/Code**	**Individual**
-	3	CSC	J. Bohn, O. Clark, J. Slager
1	-	CSC	E. Morris
3	3	PMS 385	M. Fink, D. Liese, A. Rausch
1	1	SEA 05D	S. Wynn
1	1	SEA 05	J. Schumann
1	-	DTIC	
-	1	2000	C. Dicks
-	1	2240	C. Kennell
1	1	2410	A. Anderson
1	-	2420	S. Fung
-	1	3452 (Library)	
-	1	5030	S. Jessup
1	-	5060	D. Walden
-	1	5800	T. Fu
-	3	5800	D. Cusanelli, G. Karafiath, J. Slutsky
-	1	5800	R. Hurwitz
10	**18**		